

Transit analysis of the CoRoT-5, CoRoT-8, CoRoT-12, CoRoT-18, CoRoT-20, and CoRoT-27 systems with combined ground- and space-based photometry

St. Raetz^{1,2,3*}, A. M. Heras³, M. Fernández⁴, V. Casanova⁴, C. Marka⁵

¹*Institute for Astronomy and Astrophysics Tübingen (IAAT), University of Tübingen, Sand 1, D-72076 Tübingen, Germany*

²*Freiburg Institute of Advanced Studies (FRIAS), University of Freiburg, Albertstraße 19, D-79104 Freiburg, Germany*

³*Science Support Office, Directorate of Science, European Space Research and Technology Centre (ESA/ESTEC), Keplerlaan 1, 2201 AZ Noordwijk, The Netherlands*

⁴*Instituto de Astrofísica de Andalucía, CSIC, Apdo. 3004, 18080 Granada, Spain*

⁵*Instituto Radioastronomía Milimétrica (IRAM), Avenida Divina Pastora 7, E-18012 Granada, Spain*

Accepted 2018 November 8. Received: 2018 November 7; in original form 2018 April 6

ABSTRACT

We have initiated a dedicated project to follow-up with ground-based photometry the transiting planets discovered by *CoRoT* in order to refine the orbital elements, constrain their physical parameters and search for additional bodies in the system.

From 2012 September to 2016 December we carried out 16 transit observations of six *CoRoT* planets (CoRoT-5 b, CoRoT-8 b, CoRoT-12 b, CoRoT-18 b, CoRoT-20 b, and CoRoT-27 b) at three observatories located in Germany and Spain. These observations took place between 5 and 9 yr after the planet’s discovery, which has allowed us to place stringent constraints on the planetary ephemeris. In five cases we obtained light curves with a deviation of the mid-transit time of up to ~ 115 min from the predictions. We refined the ephemeris in all these cases and reduced the uncertainties of the orbital periods by factors between 1.2 and 33. In most cases our determined physical properties for individual systems are in agreement with values reported in previous studies. In one case, CoRoT-27 b, we could not detect any transit event in the predicted transit window.

Key words: planets and satellites: individual: CoRoT-5 b, CoRoT-8 b, CoRoT-12 b, CoRoT-18 b, CoRoT-20 b, and CoRoT-27 b; planetary systems; stars: individual: CoRoT-5, CoRoT-8, CoRoT-12, CoRoT-18, CoRoT-20, and CoRoT-27 .

1 INTRODUCTION

The study of transiting extrasolar planets was revolutionized by the data obtained by space telescopes like *CoRoT* and *Kepler*, as they provide high-precision, high-cadence, continuous light curves (LCs) of a very high number of stars. Thanks to these extraordinary capabilities, the first rocky super-Earths were detected (CoRoT-7b, Kepler-10b, Queloz et al. 2009; Batalha et al. 2011), starting a new era of exoplanet discoveries.

CoRoT (convection, rotation and planetary transits) was the first space mission dedicated to the detection of transiting planets. The mission was launched in 2006 December and started its first science observation in 2007 January. The spacecraft was equipped with a 27-cm telescope and a 4-CCD wide-field camera. Each pair of CCDs was designed

for one of the two main goals of the mission, asteroseismology, or exoplanets. A complete overview on the *CoRoT* mission can be found in ‘The *CoRoT* Legacy Book: The adventure of the ultra high precision photometry from space’ (CoRoT Team 2016). Because of its low-earth orbit, *CoRoT* could point in one direction for not longer than 6 months per year to avoid the Sun entering in its field of view (FoV). The ~ 6 month observing time in one direction was divided into two separate runs lasting ~ 30 d (short run, SR) and ~ 150 d (long run, LR). *CoRoT* observed the fields with two cadence modes, a short cadence of 32 s exposure time and a long cadence with 16 exposures of 32 s stacked together resulting in 512 s cadence (Ollivier et al. 2016). While most stars were observed in long cadence mode, the 32 s exposures were only downloaded for selected targets i.e. after the detection of transit like events.

In 2009 March, the satellite suffered a loss of communication with one of the data processing units (DPU), which

* E-mail:raetz@astro.uni-tuebingen.de

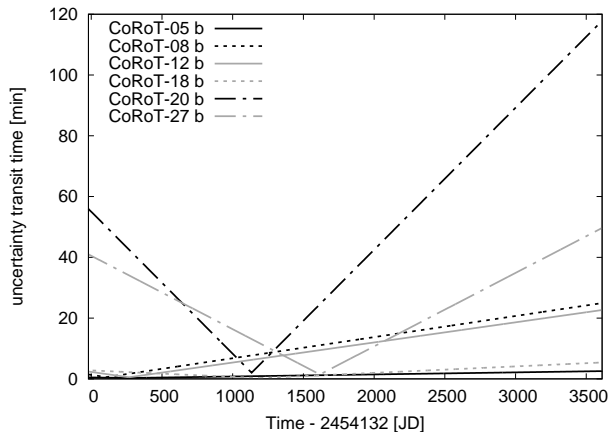


Figure 1. Propagation of the uncertainties on the original published ephemeris for our targets from the start of *CoRoT*’s first science run in 2007 January to our last observation 2016 December. The change points of the lines (close to zero) denotes the transit time at epoch zero (transit discovery).

reduced the FoV by 50%. In 2012 November, the second and last DPU failed resulting in the end of the mission in 2013 June. So far 34 confirmed exoplanets have been published and ~ 500 candidate exoplanets are awaiting evaluation (CoRoT Team 2016).

To truly benefit from *CoRoT*’s planet findings, the planet and orbit parameters need to be accurately determined. Since *CoRoT* could observe transiting planets only for a maximum duration of 150 d, ground-based follow-up is mandatory to extend the observational baseline. We have therefore initiated a dedicated project to combine the unprecedented precision of *CoRoT* LCs with ground-based follow-up photometry, in order to refine the planets orbital elements, constrain their physical parameters and search for additional bodies in the system. We selected 12 suitable targets that fulfilled the following criteria:

- The brightness of the host star is $V < 16$ mag and the transit depth is at least 8 mmag, to ensure sufficient photometric and timing precision at 1-2 m class ground-based telescopes.
- The orbit of the known transiting planet is not well constrained through radial velocity (RV) observations or shows non-zero eccentricity (though the circularization time-scale is much shorter than the system age) and/or the data presents deviant RV points, possibly indicating a perturber.
- Timing errors are critically large, which would impede the planetary transit observations within a few years.

A short description and first results of this study were published in Raetz et al. (2015). Here, we report on our observations of six of these targets, CoRoT-5, CoRoT-8, CoRoT-12, CoRoT-18, CoRoT-20, and CoRoT-27. Table 1 summarizes the literature values of the physical properties of these systems. Fig. 1 gives the propagation of the original published ephemeris uncertainties for these targets to the present. In particular, CoRoT-20 and CoRoT-27 are of special interest as they have the largest uncertainties in our sample. Moreover, both targets are massive hot Jupiters and, hence, very interesting systems to study formation, migration, and evolution of gas giant planets.

2 OBSERVATION, DATA REDUCTION, AND PHOTOMETRY

We started our follow-up campaign in 2013 October after first test observations that were carried out in 2012 September. In total, we collected 16 high-precision LCs of the six selected targets, CoRoT-5, CoRoT-8, CoRoT-12, CoRoT-18, CoRoT-20, and CoRoT-27, from 2012 September to 2016 December. Our ground-based observations were performed with three 1-m class telescopes located in Germany and Spain. Summaries of the participating observatories and observations are given in Table 2 and Table 3, respectively. We have also re-analysed the *CoRoT* observations for these targets. The details are given in the following sections.

2.1 *CoRoT* observations

We downloaded the fully reduced LCs (N2 – the primary scientific, Version 2.1 or 2.2) produced by the *CoRoT* pipeline (Auvergne et al. 2009) from the CoRoT archive mirror at the ‘NASA Exoplanet Archive’ (Akeson et al. 2013, <http://exoplanetarchive.ipac.caltech.edu/>). In all cases we used the white-light LCs. For most of the targets, the LCs consist of the long cadence data at the beginning of the observations as well as short cadence data for the rest.

In preparation for the LC analysis we applied several steps to clean the LCs. First, we removed all flagged measurements (flagged e.g. because of energetic particles, South Atlantic Anomaly crossings, Earth eclipses; Chaintreuil et al. 2016). Then we extracted the transits from the LC by using all data points ± 0.2 d around the expected transit time calculated with the published ephemeris. In the same step, we corrected the time stamp, which is given in heliocentric julian date at the end of the measurements in the original LCs, to the middle of the exposure. In step three, we normalized the LCs. After the division by the average out-of-transit flux, additional light (‘third’ light) L_3 induced by contaminants in the aperture around the target star was subtracted from the normalized flux before re-normalizing. In a last step we cleaned the LCs from outliers. By using a moving average of the time-series we created a smoothed LC. Finally, we removed all data points that deviated more than 3σ from this smoothed LC.

2.2 Ground-based observations

One observation in 2012 was carried out using the ‘Schmidt Teleskop Kamera’ (STK, Mugrauer & Berthold 2010) mounted at the 90 cm Schmidt telescope (60 cm in Schmidt mode) at the University Observatory Jena. With 2048×2048 pixels and a pixel scale of 1.55 arcsec/pixel, we could observe a large FoV of 53×53 arcmin.

Most of the LCs (12 out of 16) were collected with the 1.5-m reflector at the Observatorio de Sierra Nevada (OSN), which is operated by the Instituto de Astrofísica de Andalucía, CSIC, Spain. Using a VersArray:2048B CCD camera (2048×2048 pixels, pixel scale 0.23 arcsec/pixel) we covered a FoV of 7.85×7.85 arcmin.

From 2015 November to 2016 June we obtained three additional LCs at ESA’s Optical Ground Station (OGS), a 1-m telescope located at the Observatorio del Teide on Tenerife. The mounted spectrograph (Schulz et al. 2014) was used

Table 1. Physical and orbital properties of the observed systems summarized from the literature.

Object	CoRoT-5	CoRoT-8	CoRoT-12	CoRoT-18
Epoch zero transit time T_0 [d]	2454400.19885 [1] ± 0.00020 [1]	2454239.03311 [2] ± 0.00078 [2]	2454398.62707 [4] ± 0.00036 [4]	2455321.72412 [6] ± 0.00018 [6]
Orbital period P [d]	4.0378962 \pm 0.0000019 [2]	6.212381 \pm 0.000057 [2]	2.828042 \pm 0.000013 [4]	1.9000693 \pm 0.0000028 [6]
Semimajor axis a [au]	0.05004 \pm 0.001265 [2]	0.063 \pm 0.001 [3]	0.04016 \pm $\begin{smallmatrix} 0.00093 \\ 0.00092 \end{smallmatrix}$ [4]	0.02860 \pm 0.00065 [7]
Inclination i [°]	86.24 \pm 0.53 [2]	88.4 \pm 0.1 [3]	85.79 \pm 0.43 [2]	86.5 \pm $\begin{smallmatrix} 1.4 \\ 0.9 \end{smallmatrix}$ [6]
Eccentricity e	0.09 \pm $\begin{smallmatrix} 0.09 \\ 0.04 \end{smallmatrix}$ [1]	0* [3]	0.070 \pm $\begin{smallmatrix} 0.063 \\ 0.042 \end{smallmatrix}$ [4]	0.10 \pm 0.04 [8]
Mass star M_A [M_\odot]	1.00 \pm 0.02 [1]	0.88 \pm 0.04 [3]	1.078 \pm $\begin{smallmatrix} 0.077 \\ 0.072 \end{smallmatrix}$ [4]	0.861 \pm 0.059 [7]
Radius star R_A [R_\odot]	1.186 \pm 0.040 [1]	0.77 \pm 0.02 [3]	1.046 \pm 0.042 [2]	0.924 \pm 0.057 [7]
Effective temperature T_{eff} [K]	6100 \pm 65 [1]	5080 \pm 80 [3]	5675 \pm 80 [4]	5440 \pm 100 [6]
Surface gravity star $\log g_A$	4.19 \pm 0.03 [1]	4.58 \pm 0.08 [3]	4.375 \pm $\begin{smallmatrix} 0.065 \\ 0.062 \end{smallmatrix}$ [4]	4.442 \pm 0.043 [7]
Metallicity $\left[\frac{Fe}{H}\right]$	-0.25 \pm 0.06 [1]	0.3 \pm 0.1 [3]	0.16 \pm 0.10 [4]	-0.1 \pm 0.1 [6]
Mass planet M_b [M_{Jup}]	0.467 \pm $\begin{smallmatrix} 0.047 \\ 0.024 \end{smallmatrix}$ [1]	0.22 \pm 0.03 [3]	0.917 \pm $\begin{smallmatrix} 0.070 \\ 0.065 \end{smallmatrix}$ [4]	3.27 \pm 0.17 [7]
Radius planet R_b [R_{Jup}]	1.388 \pm $\begin{smallmatrix} 0.046 \\ 0.047 \end{smallmatrix}$ [1]	0.57 \pm 0.02 [3]	1.350 \pm 0.074 [2]	1.251 \pm 0.083 [7]
Distance [pc]		380 \pm 30 [3]	1150 \pm 85 [4]	870 \pm 90 [6]
Age [Gyr]	\sim 5.5 - 8.3 [1]	\leq 3 [3]	6.3 \pm 3.1 [4]	0.1 \pm $\begin{smallmatrix} 0.8 \\ 0.04 \end{smallmatrix}$ [6]
Spectral type	F9V [1]	K1V [3]	G2V [5]	G9V [6]
RA	06h45m07s [1]	19h26m21s [3]	06h43m04s [4]	06h32m41.36s [6]
Dec	00°48'55" [1]	01°25'36" [3]	01°17'47" [4]	-00°01'53.71" [6]
V [mag]	14.0 [1]	14.8 [3]	15.515 \pm 0.052 [4]	15.00 \pm 0.10 [6]

Object	CoRoT-20	CoRoT-27
Epoch zero transit time T_0 [d]	2455266.0001 [9] ± 0.0014 [9]	2455748.684 [10] ± 0.001 [10]
Orbital period P [d]	9.24285 \pm 0.00030 [9]	3.57532 \pm 0.00006 [10]
Semimajor axis a [au]	0.0902 \pm 0.0021 [9]	0.0476 \pm 0.0066 [10]
Inclination i [°]	88.21 \pm 0.53 [9]	86.7 \pm $\begin{smallmatrix} 1.2 \\ 0.8 \end{smallmatrix}$ [10]
Eccentricity e	0.562 \pm 0.013 [9]	<0.065 [10]
Mass star M_A [M_\odot]	1.11 \pm 0.01 [7]	1.05 \pm 0.11 [10]
Radius star R_A [R_\odot]	1.02 \pm 0.05 [9]	1.08 \pm $\begin{smallmatrix} 0.18 \\ 0.06 \end{smallmatrix}$ [10]
Effective temperature T_{eff} [K]	5880 \pm 90 [9]	5900 \pm 120 [10]
Surface gravity star $\log g_A$	4.20 \pm 0.15 [9]	4.4 \pm 0.1 [10]
Metallicity $\left[\frac{Fe}{H}\right]$	0.14 \pm 0.12 [9]	0.1 \pm 0.1 [10]
Mass planet M_b [M_{Jup}]	4.24 \pm 0.23 [9]	10.39 \pm 0.55 [10]
Radius planet R_b [R_{Jup}]	0.84 \pm 0.04 [9]	1.007 \pm 0.044 [10]
Distance [pc]	1230 \pm 120 [9]	
Age [Gyr]	0.1 \pm $\begin{smallmatrix} 0.8 \\ 0.04 \end{smallmatrix}$ [9]	4.21 \pm 2.72 [10]
Spectral type	G2V [9]	G2V [10]
RA	06h30m53s [6]	18h33m59s [10]
Dec	00°13'37" [9]	05°32'18.503" [10]
V [mag]	14.66 [9]	15.540 [10]

References: [1] Rauer et al. (2009), [2] Southworth (2011), [3] Bordé et al. (2010), [4] Gillon et al. (2010), [5] Ehrenreich & Désert (2011), [6] Hébrard et al. (2011), [7] Southworth (2012), [8] Parviainen et al. (2013), [9] Deleuil et al. (2012), [10] Parviainen et al. (2014)

*Fixed in radial velocity analysis.

Table 2. Observatories and instruments used to observe transits of the *CoRoT* targets.

Observatory	Long. (E) [°]	Lat. (N) [°]	Altitude [m]	Mirror \varnothing [m]	Camera	# Pixel	Pixel scale ["/pix]	FoV [']
Jena/Germany	11.5	50.9	370	0.90 ^a	E2V CCD42-10 (STK) ^b	2048 x 2048	1.55	52.8 x 52.8
Sierra Nevada/Spain	356.6	30.1	2896	1.50	VersArray:2048B	2048 x 2048	0.23	7.8 x 7.8
Teide/Tenerife	343.5	28.3	2390	1.00	Roper Spec Camera	2048 x 2048	0.40	13.8 x 13.8

^a0.60 m in Schmidt mode, ^b Mugrauer & Berthold (2010)

in imaging mode for the observations. The Roper Spec Camera provides 2048×2048 pixels with a pixel scale of 0.403 arcsec/pixel. The initial FoV of 13.8×13.8 arcmin was windowed to shorten read-out time.

Since the *CoRoT* targets are relatively faint ($V \sim 14 - 15.5$ mag, see Table 1) all observations were carried out either in *R*-band or without any filter, with exposure times between 90 and 180 s.

Data reduction and photometry were performed following the procedures described by us in e.g. Raetz et al. (2014, 2016). In short, we subtracted a bias (as overscan for the data of the STK) and a dark frame (only for STK) and divided by a sky flat field using the IRAF¹ routines *zerocombine*, *darkcombine*, *flatcombine*, and *ccdproc*. For the aperture photometry with 10 different aperture radii we used a script based on the standard IRAF routine *phot*. Finally, we derived differential magnitudes using an optimized artificial comparison star (Broeg et al. 2005). We chose the aperture radius that produced the lowest LC scatter (lowest standard deviation) for a sample of constant stars.

As preparation for the LC analysis we applied part of the LC treatment as explained for the *CoRoT* LCs. In particular, steps three and four were performed to transform the differential magnitudes into fluxes, normalize the LCs, and remove outliers.

3 LIGHT CURVE ANALYSIS

The LC analysis was performed by fitting the transit model of Mandel & Agol (2002) to the LCs using the Transit Analysis Package² (TAP v2.1, Gazak et al. 2012). TAP fits the LCs using EXOFAST (Eastman et al. 2013) and estimates parameter uncertainties with the wavelet-based technique of Carter & Winn (2009).

All *CoRoT* and ground-based LCs of a given target were simultaneously fitted using 10 Markov Chain Monte Carlo (MCMC) chains with 10^5 steps each. The wavelength independent parameters (orbital inclination i and the semimajor-axis scaled by stellar radius $\frac{a}{R_A}$) and the wavelength dependent parameters (planetary to stellar radii ratio $\frac{R_b}{R_A}$ and the limb darkening coefficients) were connected for all LCs and for LCs in the same filter, respectively. The signal-to-noise ratio of the individual LCs was not sufficient (between ~ 2 and 16) to derive the limb darkening coefficients from the LC analysis (Csizmadia et al. 2013). When the coefficients were allowed to vary in a wide range, the fitting procedure sometimes gave unphysical results. However, to not underestimate the parameter uncertainties by using limb darkening coefficients that were held fixed (see e.g. Maciejewski et al. 2013), they were allowed to vary ± 0.1 around the theoretical values for the quadratic limb darkening law (used by TAP). The limb darkening coefficients were inferred from the tables by Claret (2000) and Sing (2010) for the ground-based and the *CoRoT* observations, respectively. Photometric trends in the LCs were fitted simultaneously

¹ IRAF is distributed by the National Optical Astronomy Observatories, which are operated by the Association of Universities for Research in Astronomy, Inc., under cooperative agreement with the National Science Foundation.
² <http://ifa.hawaii.edu/users/zgazak/IfA/TAP.html>

Table 3. Summary of our observations at the University Observatory Jena with the STK, the Observatorio de Sierra Nevada (OSN), and ESA’s Optical Ground Station (OGS) in the period from 2012 September to 2016 December. N_{exp} : number of exposures, T_{exp} : exposure times

Date	Telescope	Filter	N_{exp}	T_{exp} [s]
CoRoT-5				
2014 Jan 07	OSN	<i>R</i>	132	120
2015 Oct 27	OSN	<i>R</i>	115	150
2016 Dec 20	OSN	<i>R</i>	123	120
CoRoT-8				
2012 Sep 06	STK	<i>R</i>	96	120
2016 Jun 16	OGS	white light	111	180,120
CoRoT-12				
2014 Dec 22	OSN	<i>R</i>	116	120,150
2015 Nov 15	OGS	white light	114	120
2016 Feb 25	OSN	<i>R</i>	83	180
CoRoT-18				
2014 Jan 20	OSN	<i>R</i>	101	120, 150
2014 Oct 28	OSN	<i>R</i>	98	150, 160
2014 Nov 16	OSN	<i>R</i>	123	140
2016 Jan 31	OSN	<i>R</i>	112	120, 130, 150
CoRoT-20				
2015 Jan 08	OSN	<i>R</i>	103	150,140
2015 Nov 18	OGS	white light	65	90
CoRoT-27				
2016 Jun 03	OSN	<i>R</i>	126	180
2016 Jun 28	OSN	<i>R</i>	100	180

with the transit. The system parameters resulting from the LC modelling are given in Table 4.

4 PHYSICAL PROPERTIES

From the system parameters we obtained from the LC modelling, we calculated the physical properties for each of the observed systems. As explained by us in detail in e.g. Raetz et al. (2015), we followed the procedures of Southworth (2009). In a first step, we determined the stellar parameters mass M_A , luminosity L_A , and age by employing PARSEC isochrones (version 1.2S, Bressan et al. 2012). For transiting planetary systems, a modified version of the Hertzsprung–Russel diagram (HRD) can be drawn by using the mean stellar density ρ_A , which can accurately be determined from the LC modelling as shown by Winn (2010). The improved orbital period P necessary to calculate ρ_A was derived from all available transit times (see the next section). In addition, we deduced the stellar radius R_A and the surface gravity g_A from the fitted parameters a/R_A and R_b/R_A and the simplified formulas given in Southworth (2009), respectively. The planetary parameters R_b and g_b were derived along with the stellar ones. In the next step, we re-determined the planetary mass M_b and computed the plan-

Table 4. System parameters resulting from the simultaneous wavelet-based red noise MCMC analysis of all *CoRoT* and ground-based LCs.

Object	CoRoT-5	CoRoT-8	CoRoT-12	CoRoT-18	CoRoT-20
Inclination [°]	85.68 ^{+0.18} _{-0.17}	86.88 ^{+0.41} _{-0.34}	85.71 ^{+0.39} _{-0.36}	89.9 ^{+1.6} _{-1.6}	85.9 ^{+2.5} _{-2.2}
a/R_A	9.54 ^{+0.20} _{-0.19}	13.7 ^{+1.0} _{-0.8}	8.02 ^{+0.26} _{-0.24}	7.013 ^{+0.078} _{-0.160}	16.5 ^{+2.0} _{-2.7}
R_b/R_A (<i>CoRoT</i> white light)	0.1155 ^{+0.0083} _{-0.0084}	0.0849 ^{+0.0020} _{-0.0022}	0.1314 ^{+0.0015} _{-0.0015}	0.1331 ^{+0.0014} _{-0.0013}	0.0884 ^{+0.0045} _{-0.0035}
R_b/R_A (<i>R</i> -band)	0.1123 ^{+0.0022} _{-0.0022}	0.081 ^{+0.011} _{-0.008}	0.1297 ^{+0.0032} _{-0.0033}	0.1410 ^{+0.0020} _{-0.0019}	0.0885 ^{+0.0066} _{-0.0065}
R_b/R_A (white light)		0.0757 ^{+0.0072} _{-0.0040}	0.1437 ^{+0.0039} _{-0.0042}		
Linear LD* (<i>CoRoT</i> white light)	0.360 ^{+0.017} _{-0.017}	0.579 ^{+0.020} _{-0.021}	0.472 ^{+0.015} _{-0.014}	0.492 ^{+0.025} _{-0.025}	0.420 ^{+0.050} _{-0.049}
Quad LD* (<i>CoRoT</i> white light)	0.271 ^{+0.018} _{-0.018}	0.129 ^{+0.021} _{-0.021}	0.211 ^{+0.015} _{-0.014}	0.199 ^{+0.026} _{-0.026}	0.239 ^{+0.050} _{-0.050}
Linear LD* (<i>R</i> -band)	0.294 ^{+0.052} _{-0.052}	0.502 ^{+0.095} _{-0.099}	0.372 ^{+0.062} _{-0.061}	0.384 ^{+0.041} _{-0.041}	0.298 ^{+0.093} _{-0.094}
Quad LD* (<i>R</i> -band)	0.398 ^{+0.053} _{-0.053}	0.227 ^{+0.097} _{-0.098}	0.322 ^{+0.065} _{-0.066}	0.292 ^{+0.047} _{-0.048}	0.335 ^{+0.096} _{-0.098}
Linear LD* (white light)		0.36 ^{+0.10} _{-0.10}	0.321 ^{+0.084} _{-0.085}		
Quad LD* (white light)		0.27 ^{+0.10} _{-0.10}	0.297 ^{+0.091} _{-0.090}		

* were allowed to vary ± 0.1 around the theoretical values (see text)

etary density ρ_b . We then calculated the planet’s equilibrium temperature, T_{eq} , assuming the effective temperature of the host star from the literature and the Safronov number Θ (a measure of the efficiency with which a planet gravitationally scatters other bodies, Safronov 1972). Finally we calculated the geometrical parameters, semimajor axis a using Kepler’s third law, and the impact parameter b .

5 TRANSIT TIMING

The mid-transit times of each transit were obtained by the simultaneous modelling with TAP where T_c was always a free parameter. The transit times, which are given in heliocentric julian date and julian date for the *CoRoT* and the ground-based observations, respectively, were converted into the barycentric Julian Date based on the barycentric dynamic time (BJD_{TDB}) using the online converter³ by Eastman et al. (2010). Our observations were carried out 5-9 yr, 7 yr on average, after the *CoRoT* planet discovery. We used the ephemeris that are available in the literature to compute ‘observed minus calculated’ (O–C) residuals for all transit times. As expected from the uncertainties of the published ephemeris, in most cases the observed transit times deviate significantly from the predicted ones. Hence, a recalculation of the transit ephemeris was necessary for all observed targets. For an exact determination of the ephemeris we plotted the mid-transit times over the epoch and performed a weighted linear fit.

Finally, we computed the generalized Lomb–Scargle periodogram (GLS; Zechmeister & Kürster 2009) to search for a periodicity in the transit timing residuals.

6 COROT-5

CoRoT-5 b was discovered during the first LR on the galactic anti-centre direction (LRa01) that started on 2007 October 24 and lasted 112 d (Rauer et al. 2009). The observations started with a cadence of 512s that was changed to the 32s-mode after seven transit events. In total, 31 transits were

found. One event was lost in a larger data gap caused by a DPU reset (Rauer et al. 2009). Photometric and spectroscopic follow-up observations were scheduled right after the ‘‘alarm mode’’ was triggered. Radial velocity measurement with SOPHIE and HARPS confirmed that CoRoT-5 b is a hot Jupiter-type planet orbiting a 14 mag F9V star. The spectroscopic observations also yielded a slight eccentricity of the planetary orbit. The published physical properties of the CoRoT-5 system are summarized in Table 1. CoRoT-5 b belongs to the planets with the lowest mean density. It was found to be larger by 20% compared to standard evolutionary models (Rauer et al. 2009).

We observed three ground-based LCs between 2014 January and 2016 December at OSN. The exposure times of the *R*-band observations were chosen between 120 and 150 s.

We also re-analysed the *CoRoT* data that initially consisted of 269 390 data points. After removing all flagged data the number of data points reduced to 236 774. We extracted 31 transit events with a depth of $\sim 1.4\%$ and a duration of ~ 2.7 h. The contribution of L_3 was estimated to be 8.4% by Rauer et al. (2009).

The ground-based LCs together with the best-fitting model is shown in Fig. 2. We have also plotted the transit times into an O–C diagram. Our ground-based observations deviate up to ~ 20 min from the predicted transit times, while the uncertainties on the original ephemeris estimated a shift of only ~ 2.5 min. Since an accurate determination of the ephemeris is hindered by the short time span of the *CoRoT* observations, the uncertainties on the original ephemeris might have been underestimated. An alternative explanation for the deviation of one order of magnitude more than predicted could be the presence of significant transit timing variations (TTVs). This is, however, not supported by our observations. The result of our re-determined ephemeris is given in equation 1, where E denotes the epoch ($\chi^2 = 8.8$, reduced $\chi^2 = 0.27$):

$$T_{c[\text{BJD}_{\text{TDB}}]}(E) = (2454400.19896 \pm 0.00022 + E \cdot 4.0379156 \pm 0.0000012) \text{ d} \quad (1)$$

The updated version of the O–C diagram as well as all transit times and the corresponding O–C values are given in Fig. 3 and Table 5, respectively. We could not find any periodic signal in the transit times. The highest

³ <http://astrutils.astronomy.ohio-state.edu/time/utc2bjd.html>

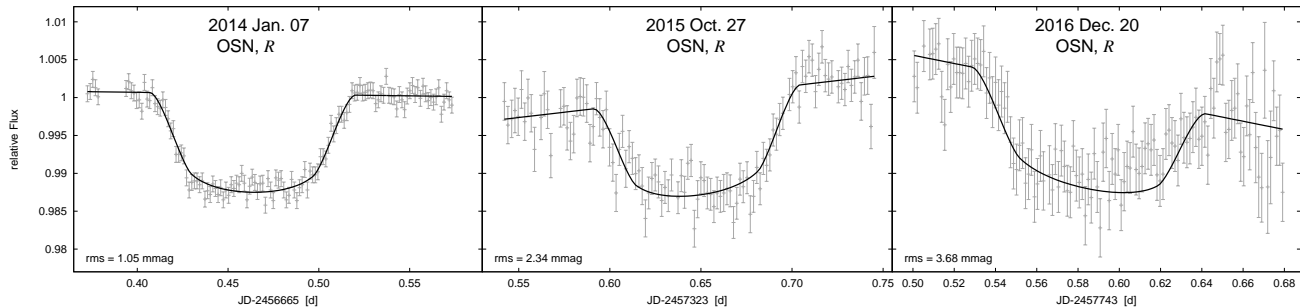


Figure 2. Light curves of CoRoT-5 b with best-fitting model resulting from the simultaneous fit of all *CoRoT* and ground-based LCs. The dates of observation, observatory, filter, and the *rms* of the fit are indicated in each individual panel.

peak in the periodogram obtained with GLS at a period of $P_{\text{TTV}} = 90.0 \pm 0.8$ epochs shows a false-alarm-probability (FAP) of 99.9%. The asymmetric shape of our LC from 2016 Dec. 20 could be an indication of stellar activity. Large spots are, however, unlikely as CoRoT-5 does not show strong out of transit variability (Rauer et al. 2009). We cannot discard that the CoRoT observations were taken during a minimum of the stellar activity cycle, and the ground-based observations are carried out during a maximum. Further high-precision photometric follow-up observations would be necessary to confirm stellar activity.

The results of the LC analysis is given in Table 4 and shown in Fig. 4, the obtained physical properties are summarized in Table 6. We found the geometrical parameters in excellent agreement with the ones of Rauer et al. (2009). Also most of the stellar and planetary values agree with each other within their error bars on a 2σ level. Only the surface gravity of the star that was determined spectroscopically in Rauer et al. (2009) slightly differs. These authors also give the photometrically obtained value of $\log g_A = 4.311 \pm 0.033$, which agrees with the result of our LC analysis.

Fig. 5 shows the position of CoRoT-5 in a modified version of the HRD, together with the PARSEC isochrones. CoRoT-5 is in an area of the HRD with overlapping isochrones of young (~ 20 Myr) and old (~ 6 Gyr) ages. However, as Rauer et al. (2009) have already shown, the very low level of stellar variability in the global LC as well as the missing signs of the CaII or a strong LiI absorption line hints to the older age.

7 COROT-8

CoRoT-8b, which was observed by *CoRoT* during the first LR in constellation Aquila (LRc01) from 2007 May 16 to October 5, orbits a K1 dwarf in ~ 6.2 d (Bordé et al. 2010). It was detected by the ‘alarm mode’-pipeline which switched the observation mode to the short cadence after ~ 68 d and triggered follow-up observations. L_3 is given as 1.55% in the *Exo-dat* data base (Deleuil et al. 2009). RV follow-up observations that confirmed the planetary nature of CoRoT-8b were carried out with SOPHIE and HARPS. With its measured radius and mass, CoRoT-8b appears to be somewhat between Saturn and Neptune (Bordé et al. 2010).

We observed two transits of CoRoT-8 separated by ~ 4 yr. One transit was observed in 2012 September 6 at the University Observatory Jena and the other one in 2016 June 16

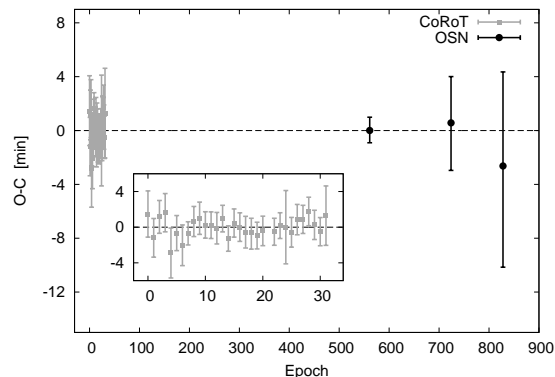


Figure 3. The O–C diagram of CoRoT-5 b. The grey squares and the black circles denote the *CoRoT* and the OSN transits, respectively. The dashed line represents the updated ephemeris given in equation 1.

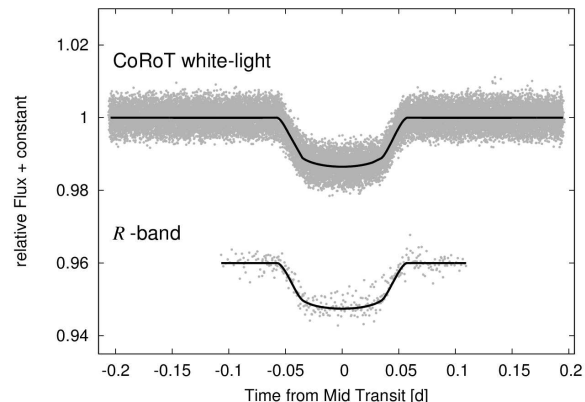


Figure 4. Phase-folded LCs of all 31 *CoRoT* transits as well as of all three OSN *R*-band transits of CoRoT-5. The trend was removed before phase-folding. Overlaid are the best-fitting models obtained with TAP.

at ESA’s OGS. Unfortunately, in both cases we could only observe a partial transit event. Our LCs are shown in Fig. 6. We extracted 23 transits, 11 of them in long cadence mode, from the *CoRoT*-LC that consist in total of 182 380 unflagged data points. The altogether 25 transits were simultaneously modelled. The phase-folded LCs including all transits are shown in Fig. 7. The resulting system parameters are given in Table 4.

Computing the physical properties of the system from these

Table 5. Transit times for all observed transits of CoRoT-5 b including the re-analysed *CoRoT* transits. The O–C was calculated with the ephemeris given in equation 1.

Telescope	Epoch	T_c [BJD _{TDB}]	O–C [min]
CoRoT	0	2454400.1999 ± 0.0018	1.42 ± 2.65
CoRoT	1	2454404.2360 ± 0.0015	-1.19 ± 2.17
CoRoT	2	2454408.2756 ± 0.0013	1.17 ± 1.83
CoRoT	3	2454412.3138 ± 0.0015	1.62 ± 2.16
CoRoT	4	2454416.3486 ± 0.0019	-2.85 ± 2.75
CoRoT	5	2454420.3881 ± 0.0014	-0.65 ± 1.96
CoRoT	6	2454424.4250 ± 0.0016	-2.08 ± 2.33
CoRoT	7	2454428.4639 ± 0.0009	-0.69 ± 1.30
CoRoT	8	2454432.5027 ± 0.0012	0.63 ± 1.70
CoRoT	9	2454436.5409 ± 0.0013	0.99 ± 1.82
CoRoT	10	2454440.5783 ± 0.0010	0.22 ± 1.51
CoRoT	11	2454444.6162 ± 0.0010	0.22 ± 1.50
CoRoT	12	2454448.6538 ± 0.0013	-0.14 ± 1.80
CoRoT	13	2454452.6925 ± 0.0010	0.96 ± 1.50
CoRoT	14	2454456.7289 ± 0.0010	-1.25 ± 1.40
CoRoT	15	2454460.7680 ± 0.0011	0.45 ± 1.60
CoRoT	16	2454464.8056 ± 0.0011	0.01 ± 1.61
CoRoT	17	2454468.8431 ± 0.0012	-0.56 ± 1.78
CoRoT	18	2454472.8810 ± 0.0013	-0.64 ± 1.65
CoRoT	19	2454476.9187 ± 0.0010	-0.94 ± 1.50
CoRoT	20	2454480.9570 ± 0.0011	-0.42 ± 1.65
CoRoT	22	2454489.0327 ± 0.0012	-0.53 ± 1.66
CoRoT	23	2454493.0712 ± 0.0010	0.21 ± 1.53
CoRoT	24	2454497.1089 ± 0.0028	0.02 ± 4.10
CoRoT	25	2454501.1465 ± 0.0029	0.02 ± 4.13
CoRoT	26	2454505.1854 ± 0.0012	-0.57 ± 1.67
CoRoT	27	2454509.2233 ± 0.0012	0.85 ± 1.71
CoRoT	28	2454513.2618 ± 0.0011	0.87 ± 1.59
CoRoT	29	2454517.2987 ± 0.0011	1.74 ± 1.58
CoRoT	30	2454521.3361 ± 0.0011	1.74 ± 1.63
CoRoT	31	2454525.3752 ± 0.0012	0.30 ± 1.57
OSN	561	2456665.4696 ± 0.0023	1.27 ± 3.36
OSN	724	2457323.6502 ± 0.0023	1.27 ± 3.31
OSN	828	2457743.5912 ± 0.0023	1.27 ± 3.36
OSN			0.00 ± 0.99
OSN			0.00 ± 0.91
OSN			0.57 ± 3.44
OSN			0.57 ± 3.53
OSN			-2.63 ± 6.99
OSN			-2.63 ± 7.52

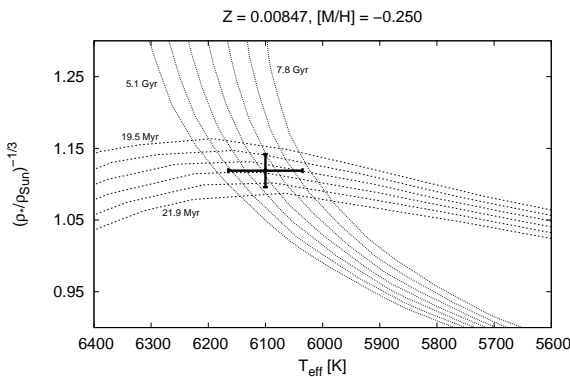

Figure 5. Position of CoRoT-5 in the $\rho_A^{-1/3} - T_{\text{eff}}$ plane. The PARSEC isochrones of metallicity $[M/H] = -0.25$ for $\log(\text{age}) = 7.29 - 7.34$ with steps of 0.01 and $\log(\text{age}) = 9.71 - 9.89$ with steps of 0.03 for the young and the old age, respectively, are also shown.

Table 6. Physical properties of the CoRoT-5 system derived from LC modelling. Values derived by Rauer et al. (2009, R09) and Southworth (2011, S11) are given for comparison.

Parameter	This work	R09	S11
Planetary parameters			
R_b [R_{Jup}]	1.256 ± 0.046	1.388 ± 0.046	1.182 ± 0.102
M_b [M_{Jup}]	0.459 ± 0.053	0.467 ± 0.047	0.470 ± 0.058
ρ_b [ρ_{Jup}]	0.217 ± 0.035	0.163 ± 0.023	0.266 ± 0.082
$\log g_b$	2.86 ± 0.05	2.89 ± 0.08	2.92 ± 0.09
T_{eq} [K]	1397 ± 15	1438 ± 38	1348 ± 50
Θ	0.0366 ± 0.0051		0.0388 ± 0.0054
Stellar parameters			
R_A [R_{\odot}]	1.115 ± 0.035	1.186 ± 0.04	1.052 ± 0.081
M_A [M_{\odot}]	0.99 ± 0.07	1.00 ± 0.02	1.025 ± 0.100
ρ_A [ρ_{\odot}]	0.714 ± 0.045		0.88 ± 0.21
$\log g_A$	4.339 ± 0.020	4.19 ± 0.03	4.405 ± 0.059
$\log \frac{L_A}{L_{\odot}}$	0.18 ± 0.05		0.16 ± 0.08
$\log(\text{Age})$	7.31 ± 0.03	$9.74 - 9.92$	
	9.80 ± 0.12		
Geometrical parameters			
a [au]	0.0495	0.04947	0.0500
	± 0.0012	± 0.00026	± 0.0016
i [$^{\circ}$]	85.68 ± 0.18	85.83 ± 0.99	86.24 ± 0.53
b	0.76 ± 0.05	0.755 ± 0.017	
	± 0.04	± 0.022	

system parameters resulted in significant deviations from the values given in Bordé et al. (2010). In particular, the stellar radius $R_A = 1.048 \pm 0.082$ R_{\odot} , the stellar density $\rho_A = 0.89 \pm 0.15$ ρ_{\odot} and the impact parameter $b = 0.75 \pm 0.09$ differ by more than 3σ . The much lower density results in a higher stellar mass and a very low pre-main-sequence age of $\log(\text{age}) = 7.38 \pm 0.13$ when plotting it into the modified HRD with the PARSEC isochrones. Consequently, also the planetary parameters deviate. The discrepancies originate in the best-fitting values of i , a/R_A and R_b/R_A obtained with TAP, which we found to be strongly correlated. The analysis of relations between the parameters reveals significant correlation or anti-correlations (with the Pearson correlation coefficients r ranging from 0.873 to 0.995) between i and a/R_A , i and R_b/R_A , and a/R_A and R_b/R_A . An example for the correlation between i and a/R_A is shown in Fig. 8. CoRoT-8 was found to be a K1 main-sequence star by (Bordé et al. 2010). They excluded very young ages because of its slow rotation and the absence of detectable CaII or LiI absorption lines. Hence, a radius of $\sim 1 R_{\odot}$ is very unlikely. A cross-check with Gaia DR2 yielded a radius of 0.8 (0.71–0.87) R_{\odot} (Gaia Collaboration et al. 2016, 2018, note: this value has to be taken with caution). Because of the strong parameter correlations a smaller radius (a higher a/R_A) can be accounted for with a higher inclination i without degrading the quality of the fit. Therefore, we placed a prior before we re-fit our data. Bordé et al. (2010) determined a projected stellar rotational velocity of $v \sin i = 2 \pm 1 \text{ km s}^{-1}$. Using the gyrochronology relation by Angus et al. (2015) and assuming spin-orbit alignment

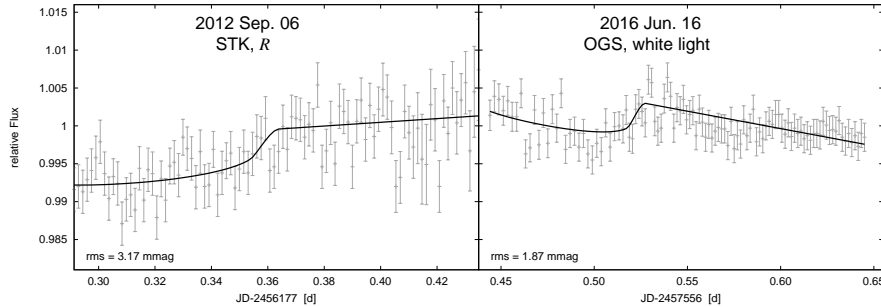


Figure 6. Same as Fig. 2 but for CoRoT-8. The date of observation, observatory, filter, and the rms of the fit are indicated in each individual panel.

Table 7. System parameters for CoRoT-8 resulting from the LC analysis with TAP. Unlike the values in Table 4, a/R_A was only allowed to vary around the value derived from a prior on the stellar density, under the Gaussian penalty defined by the derived error.

Parameter	Value
Inclination [°]	88.178 ± 0.083
a/R_A ^a	17.05 ± 0.16
R_b/R_A (CoRoT white light)	0.07915 ± 0.00099
R_b/R_A (R-band)	0.072 ± 0.0120
R_b/R_A (white light)	0.0691 ± 0.0081
Linear LD ^b (CoRoT white light)	0.583 ± 0.021
Quad LD ^b (CoRoT white light)	0.133 ± 0.021
Linear LD ^b (R-band)	0.498 ± 0.020
Quad LD ^b (R-band)	0.226 ± 0.094
Linear LD ^b (white light)	0.36 ± 0.098
Quad LD ^b (white light)	0.271 ± 0.098

^a was allowed to vary within a prior

^b were allowed to vary ± 0.1 around the theoretical values

($i \sim 90^\circ$), we estimated a stellar age of $1.7 \pm_{-1.4}^{+2.3}$ Gyr. The PARSEC isochrones of our age estimate were used to constrain the stellar density to $\rho_A = 1.73 \pm 0.26 \rho_\odot$. The resulting value of $a/R_A = 17.07 \pm 0.84$ (calculated by using the formula of Winn 2010) was finally used as prior for the LC modelling with TAP. The results of our re-analysis using a prior on the stellar density are given in Table 7, and the corresponding physical properties of the system in comparison to the literature values are summarized in Table 8. By applying gyrochronology to constrain the stellar density we found the physical properties in good agreement (on a $2\text{-}\sigma$ level) with the values of Bordé et al. (2010). However, using a prior in the fitting process may result in our uncertainties being underestimated.

Although with large uncertainties in the transit times because of the partial transit coverage, our measurements deviate by up to 49 min in the O–C diagram from the ephemeris given in Southworth (2011), which is larger than the estimated uncertainty (see Fig. 1). Hence, we re-determined the ephemeris. The result is given in equation 2 ($\chi^2 = 14.6$, reduced $\chi^2 = 0.63$):

$$T_{c[\text{BJD}_{\text{TDB}}]}(E) = (2454239.03317 + E \cdot 6.212445) \text{ d} \pm 0.00049 \pm 0.000007 \quad (2)$$

The updated O–C diagram is shown in Fig. 9, and all transit times and O–C values are given in Table 9. Our

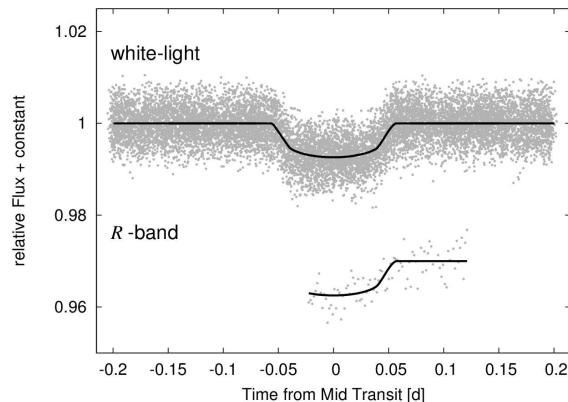


Figure 7. Phase-folded LCs of all 23 *CoRoT* transits as well as our own transits of CoRoT-8. The trend was removed before phase-folding. Overlaid are the best-fitting models obtained with TAP.

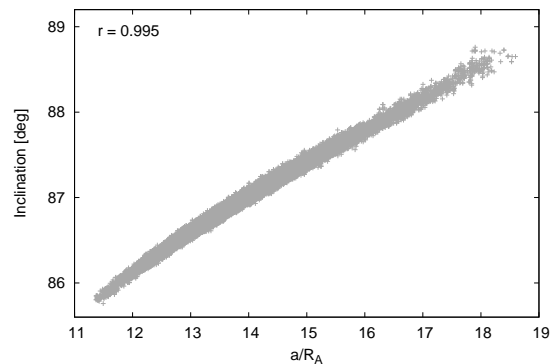


Figure 8. Example of a significant correlation between a/R_A and the orbital inclination i (correlation coefficients $r = 0.995$) of CoRoT-8 b for one MCMC chain.

measurements are in very good agreement with the refined ephemeris. Bordé et al. (2010) detected statistically significant TTVs within the *CoRoT*-LC with a period of ~ 7 Epochs (~ 43.5 d). They claimed that, since it is close to a multiple of the stellar rotation period of ~ 20 d, the TTVs are induced by the stellar activity. With our analysis we cannot confirm these variations. Our period search in the O–C values with GLS showed no significant signal. The highest peak with a period of $P_{\text{TTV}} = 101.3 \pm 1.5$ epochs shows a FAP of 99.99%.

Table 8. Physical properties of the *CoRoT*-8 system derived from the results of the LC modelling given in Table 7 based on constraints on the stellar density. Values derived by Bordé et al. (2010, B10) and Southworth (2011, S11) are given for comparison.

Parameter	This work	B10	S11
Planetary parameters			
R_b [R _{Jup}]	$0.619 \pm \begin{smallmatrix} 0.016 \\ 0.017 \end{smallmatrix}$	0.57 ± 0.02	0.712 ± 0.083
M_b [M _{Jup}]	$0.218 \pm \begin{smallmatrix} 0.034 \\ 0.034 \end{smallmatrix}$	0.22 ± 0.03	0.216 ± 0.036
ρ_b [ρ_{Jup}]	$0.86 \pm \begin{smallmatrix} 0.15 \\ 0.15 \end{smallmatrix}$	1.20 ± 0.08	0.56 ± 0.21
$\log g_b$	$3.15 \pm \begin{smallmatrix} 0.07 \\ 0.07 \end{smallmatrix}$		3.03 ± 0.12
T_{eq} [K]	$870 \pm \begin{smallmatrix} 14 \\ 14 \end{smallmatrix}$		922 ± 41
Θ	$0.0503 \pm \begin{smallmatrix} 0.0083 \\ 0.0083 \end{smallmatrix}$		0.0437 ± 0.0084
Stellar parameters			
R_A [R _⊙]	$0.802 \pm \begin{smallmatrix} 0.014 \\ 0.014 \end{smallmatrix}$	0.77 ± 0.02	0.898 ± 0.090
M_A [M _⊙]	0.89 ± 0.04	0.88 ± 0.04	0.878 ± 0.078
ρ_A [ρ_{\odot}]	$1.73 \pm \begin{smallmatrix} 0.26 \\ 0.26 \end{smallmatrix}$	1.91 ± 0.07	1.21 ± 0.32
$\log g_A$	$4.58 \pm \begin{smallmatrix} 0.01 \\ 0.01 \end{smallmatrix}$	4.58 ± 0.08	4.475 ± 0.077
$\log \frac{L_A}{L_{\odot}}$	-0.40 ± 0.05		
$\log(\text{Age})$	$9.23 \pm \begin{smallmatrix} 0.37^* \\ 0.75 \end{smallmatrix}$	≤ 9.48	unconstrained
Geometrical parameters			
a [au]	0.0636 ± 0.0014	0.063 ± 0.001	0.0633 ± 0.0019
i [°]	$88.18 \pm \begin{smallmatrix} 0.08 \\ 0.08 \end{smallmatrix}$	88.4 ± 0.1	87.44 ± 0.56
b	$0.54 \pm \begin{smallmatrix} 0.03 \\ 0.02 \end{smallmatrix}$	0.49 ± 0.04	

* determined by gyrochronology

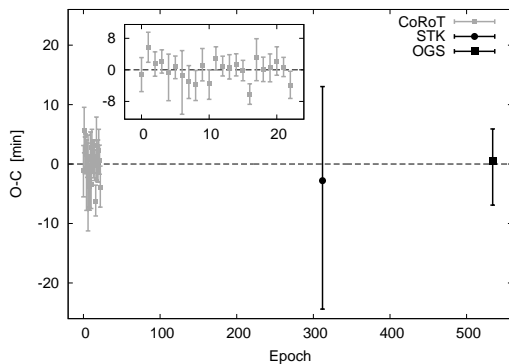


Figure 9. Same as Fig. 3 but for *CoRoT*-8b. The dashed line represents the updated ephemeris given in equation 2.

8 COROT-12

CoRoT-12b is a hot Jupiter that orbits its $V=15.5$ mag, quiet and slowly rotating star in 2.83 d. It was discovered by the *CoRoT* satellite in field LRA01 which was monitored from 2007 October 24 to 2008 March 3. The transits were noticed by the ‘alarm mode’-pipeline after 29 d of observations. L_3 was determined through ground based photometric follow-up observations as $3.3 \pm 0.5\%$. RV measurements were obtained with HARPS and with HIRES. *CoRoT*-12b appears to be a very low-density, inflated hot Jupiter. The slightly non-zero eccentricity was measured to be between 0.06 and 0.08. The *CoRoT*-LC consist of 245 780 unflagged measurements and contains 47 transits, 36 of them in the

Table 9. Same as Table 5 but for all transits of *CoRoT*-8b. The O–C was calculated with the ephemeris given in equation 2.

Telescope	Epoch	T_c [BJD _{TDB}]	O–C [min]
<i>CoRoT</i>	0	$2454239.0324 \pm \begin{smallmatrix} 0.0029 \\ 0.0031 \end{smallmatrix}$	$-1.06 \pm \begin{smallmatrix} 4.18 \\ 4.46 \end{smallmatrix}$
<i>CoRoT</i>	1	$2454245.2495 \pm \begin{smallmatrix} 0.0027 \\ 0.0026 \end{smallmatrix}$	$5.65 \pm \begin{smallmatrix} 3.89 \\ 3.74 \end{smallmatrix}$
<i>CoRoT</i>	2	$2454251.4591 \pm \begin{smallmatrix} 0.0021 \\ 0.0022 \end{smallmatrix}$	$1.55 \pm \begin{smallmatrix} 3.02 \\ 3.17 \end{smallmatrix}$
<i>CoRoT</i>	3	$2454257.6720 \pm \begin{smallmatrix} 0.0020 \\ 0.0021 \end{smallmatrix}$	$2.20 \pm \begin{smallmatrix} 2.88 \\ 3.02 \end{smallmatrix}$
<i>CoRoT</i>	4	$2454263.8824 \pm \begin{smallmatrix} 0.0033 \\ 0.0049 \end{smallmatrix}$	$-0.74 \pm \begin{smallmatrix} 4.75 \\ 7.06 \end{smallmatrix}$
<i>CoRoT</i>	5	$2454270.0959 \pm \begin{smallmatrix} 0.0019 \\ 0.0021 \end{smallmatrix}$	$0.78 \pm \begin{smallmatrix} 2.74 \\ 3.02 \end{smallmatrix}$
<i>CoRoT</i>	6	$2454276.3069 \pm \begin{smallmatrix} 0.0043 \\ 0.0069 \end{smallmatrix}$	$-1.31 \pm \begin{smallmatrix} 1.19 \\ 9.94 \end{smallmatrix}$
<i>CoRoT</i>	7	$2454282.5182 \pm \begin{smallmatrix} 0.0028 \\ 0.0030 \end{smallmatrix}$	$-2.95 \pm \begin{smallmatrix} 4.03 \\ 4.32 \end{smallmatrix}$
<i>CoRoT</i>	8	$2454288.7301 \pm \begin{smallmatrix} 0.0025 \\ 0.0028 \end{smallmatrix}$	$-3.74 \pm \begin{smallmatrix} 3.60 \\ 4.03 \end{smallmatrix}$
<i>CoRoT</i>	9	$2454294.9460 \pm \begin{smallmatrix} 0.0029 \\ 0.0028 \end{smallmatrix}$	$1.23 \pm \begin{smallmatrix} 4.18 \\ 4.03 \end{smallmatrix}$
<i>CoRoT</i>	10	$2454301.1552 \pm \begin{smallmatrix} 0.0024 \\ 0.0028 \end{smallmatrix}$	$-3.44 \pm \begin{smallmatrix} 3.46 \\ 4.03 \end{smallmatrix}$
<i>CoRoT</i>	11	$2454307.3720 \pm \begin{smallmatrix} 0.0021 \\ 0.0020 \end{smallmatrix}$	$2.83 \pm \begin{smallmatrix} 3.02 \\ 2.88 \end{smallmatrix}$
<i>CoRoT</i>	12	$2454313.5831 \pm \begin{smallmatrix} 0.0018 \\ 0.0017 \end{smallmatrix}$	$0.89 \pm \begin{smallmatrix} 2.59 \\ 2.45 \end{smallmatrix}$
<i>CoRoT</i>	13	$2454319.7954 \pm \begin{smallmatrix} 0.0022 \\ 0.0021 \end{smallmatrix}$	$0.69 \pm \begin{smallmatrix} 3.17 \\ 3.02 \end{smallmatrix}$
<i>CoRoT</i>	14	$2454326.0083 \pm \begin{smallmatrix} 0.0019 \\ 0.0020 \end{smallmatrix}$	$1.34 \pm \begin{smallmatrix} 2.74 \\ 2.88 \end{smallmatrix}$
<i>CoRoT</i>	15	$2454332.2197 \pm \begin{smallmatrix} 0.0018 \\ 0.0018 \end{smallmatrix}$	$-0.17 \pm \begin{smallmatrix} 2.59 \\ 2.59 \end{smallmatrix}$
<i>CoRoT</i>	16	$2454338.4279 \pm \begin{smallmatrix} 0.0019 \\ 0.0017 \end{smallmatrix}$	$-6.28 \pm \begin{smallmatrix} 2.74 \\ 2.45 \end{smallmatrix}$
<i>CoRoT</i>	17	$2454344.6469 \pm \begin{smallmatrix} 0.0033 \\ 0.0041 \end{smallmatrix}$	$3.16 \pm \begin{smallmatrix} 4.75 \\ 5.90 \end{smallmatrix}$
<i>CoRoT</i>	18	$2454350.8573 \pm \begin{smallmatrix} 0.0021 \\ 0.0022 \end{smallmatrix}$	$0.21 \pm \begin{smallmatrix} 3.02 \\ 3.17 \end{smallmatrix}$
<i>CoRoT</i>	19	$2454357.0700 \pm \begin{smallmatrix} 0.0024 \\ 0.0025 \end{smallmatrix}$	$0.58 \pm \begin{smallmatrix} 3.46 \\ 3.60 \end{smallmatrix}$
<i>CoRoT</i>	20	$2454363.2836 \pm \begin{smallmatrix} 0.0025 \\ 0.0025 \end{smallmatrix}$	$2.24 \pm \begin{smallmatrix} 3.60 \\ 3.60 \end{smallmatrix}$
<i>CoRoT</i>	21	$2454369.4949 \pm \begin{smallmatrix} 0.0018 \\ 0.0016 \end{smallmatrix}$	$0.59 \pm \begin{smallmatrix} 2.59 \\ 2.30 \end{smallmatrix}$
<i>CoRoT</i>	22	$2454375.7042 \pm \begin{smallmatrix} 0.0025 \\ 0.0025 \end{smallmatrix}$	$-3.94 \pm \begin{smallmatrix} 3.60 \\ 3.31 \end{smallmatrix}$
STK	312	$2456177.3142 \pm \begin{smallmatrix} 0.0110 \\ 0.0150 \end{smallmatrix}$	$-2.80 \pm \begin{smallmatrix} 15.84 \\ 21.60 \end{smallmatrix}$
OGS	534	$2457556.4794 \pm \begin{smallmatrix} 0.0037 \\ 0.0052 \end{smallmatrix}$	$0.58 \pm \begin{smallmatrix} 5.33 \\ 7.49 \end{smallmatrix}$

short cadence mode.

We observed three transits of *CoRoT*-12b from 2014 December to 2016 February, one at OSN and two at ESA’s OGS. All three LCs together with the best-fitting model are shown in Fig. 10.

The simultaneous fit of all *CoRoT* and ground-based LCs (see Fig. 11) resulted in the system parameters given in Table 4. We calculated the stellar density and plotted *CoRoT*-12 in the $\rho_A^{-1/3} - T_{\text{eff}}$ plane together with the PARSEC isochrones (Fig. 12). As already mentioned by Gillon et al. (2010) the age is poorly constrained. The modified HR-diagram shows overlapping isochrones of young and an old age. But since *CoRoT*-12 appears to be very quiet and does not show chromospheric activity or a Li absorption line, a young age seems to be unlikely. Our derived old age of $\log(\text{Age}) = 9.79 \pm 0.26$ is in agreement with the age given in Gillon et al. (2010).

As shown in Table 10, our derived physical properties of the *CoRoT*-12 system are in excellent agreement with the values in Gillon et al. (2010) and Southworth (2011). The transit times were used to refine the orbital ephemeris. The result is given in equation 3 ($\chi^2 = 26.2$, reduced $\chi^2 = 0.55$):

$$T_{c[\text{BJD}_{\text{TDB}}]}(E) = (2454398.62771 + E \cdot 2.82805268) \text{ d} \pm \begin{smallmatrix} 0.00024 \\ \pm 0.00000065 \end{smallmatrix} \quad (3)$$

The transit times and the O–C values are given in Table 11 while Fig. 13 shows the O–C diagram calculated using the updated ephemeris. The orbital period determined by Gillon et al. (2010) seems to be very accurate. We found a value that is less than a second higher but ~ 20 times more

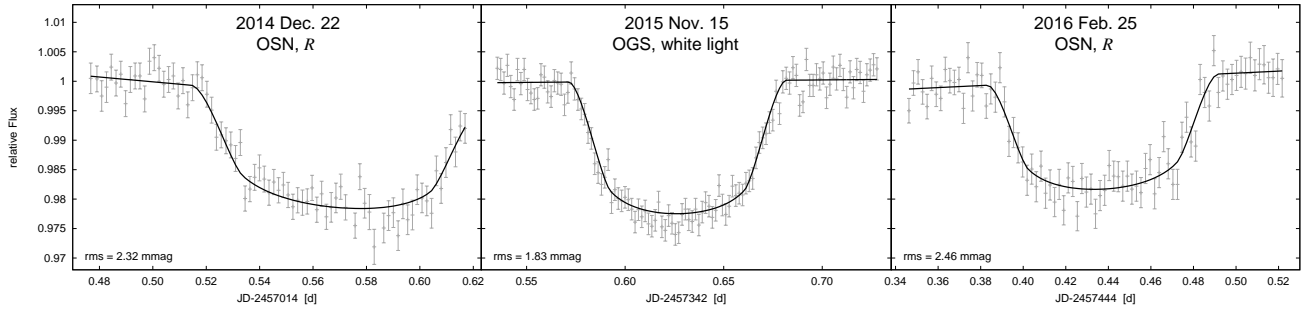


Figure 10. Same as Fig. 2 but for CoRoT-12. The date of observation, observatory, filter, and the *rms* of the fit are indicated in each individual panel.

Table 10. Same as Table 6 but for the CoRoT-12 system. Values derived by Gillon et al. (2010, G10) and Southworth (2011, S11) are given for comparison.

Parameter	This work	G10	S11
Planetary parameters			
R_b [R_{Jup}]	1.344 ± 0.074 <small>0.071</small>	1.44 ± 0.13	1.350 ± 0.074
M_b [M_{Jup}]	0.873 ± 0.081 <small>0.078</small>	0.917 ± 0.070 <small>0.065</small>	0.887 ± 0.077
ρ_b [ρ_{Jup}]	0.337 ± 0.064 <small>0.062</small>	0.309 ± 0.097 <small>0.071</small>	0.337 ± 0.052
$\log g_b$	3.080 ± 0.047 <small>0.044</small>	3.043 ± 0.082 <small>0.080</small>	3.083 ± 0.047
T_{eq} [K]	1417 ± 20 <small>20</small>	1442 ± 58	1410 ± 28
Θ	0.0509 ± 0.0073 <small>0.0071</small>		0.0508 ± 0.0042
Stellar parameters			
R_A [R_\odot]	1.049 ± 0.049 <small>0.047</small>	1.116 ± 0.096 <small>0.092</small>	1.046 ± 0.042
M_A [M_\odot]	1.00 ± 0.10	1.078 ± 0.077 <small>0.072</small>	1.018 ± 0.088
ρ_A [ρ_\odot]	0.866 ± 0.084 <small>0.078</small>	0.77 ± 0.20 <small>0.15</small>	0.889 ± 0.076
$\log g_A$	4.396 ± 0.032 <small>0.030</small>	4.375 ± 0.065 <small>0.062</small>	4.407 ± 0.029
$\log \frac{L_A}{L_\odot}$	0.01 ± 0.07		
$\log(\text{Age})$	7.43 ± 0.06	9.79 ± 0.26	9.80 ± 0.17 <small>0.29</small>
Geometrical parameters			
a [au]	0.0392 <small>± 0.0013</small>	0.04016 <small>± 0.00093 <small>0.00092</small></small>	0.0394 <small>± 0.0011</small>
i [$^\circ$]	85.71 ± 0.39 <small>0.36</small>	85.48 ± 0.72 <small>0.77</small>	85.79 ± 0.43
b	0.604 ± 0.060 <small>0.057</small>	0.573 ± 0.027 <small>0.030</small>	

precise. Although the O–C diagram of CoRoT-12 seems to show a correlated structure that was also mentioned by Gillon et al. (2010), the period search with GLS resulted in no significant detection of TTVs. The highest peak in the periodogram with a period of $P_{TTV} = 501 \pm 18$ epochs shows a FAP of 99.2%. Gillon et al. (2010) speculated that the structured O–C diagram may be caused by stellar rotation which could not be constrained from the *CoRoT* photometry.

9 COROT-18

CoRoT-18 b was detected in the field SRa03 that was observed by *CoRoT* from 2010 March 5 to 29 (Hébrard et al. 2011). It is a massive hot Jupiter that orbits its G9V host star in ~ 1.9 d. Its eccentricity is slightly non-zero ($e < 0.08$)

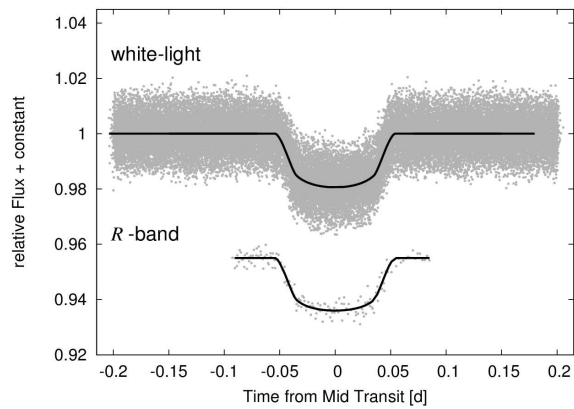


Figure 11. Phase-folded LCs of all 47 *CoRoT* transits as well as our own transits of CoRoT-12. The trend was removed before phase-folding. Overlaid are the best-fitting models obtained with TAP.

and therefore the planet also belongs to the group of massive planets on elliptical orbits. Parviainen et al. (2013) reported a statistically marginal detection of a secondary eclipse near a phase of 0.47 which corresponds to $e = 0.10 \pm 0.04$, and, hence, confirms the non-zero eccentricity. The ground-based LC of CoRoT-18 presented in Hébrard et al. (2011) revealed a brightness bump in-transit that could arise from a starspot crossing, therefore supporting the hypothesis of CoRoT-18 being a young star. However, the analysis of CoRoT-18 yielded inconsistent age determinations. While the stellar activity, lithium abundance, and stellar spin point to a young age, the evolutionary tracks do not exclude very old ages.

Based on lucky imaging observations in two different filters, Evans et al. (2016) suggested the existence of a possible companion candidate to CoRoT-18 at a separation of at least 8000 au. No definitive conclusion could be drawn due to large measurement uncertainties.

The cadence of the *CoRoT* measurements was 32 s throughout the observations. After removing all flagged entries we were left with 56 823 data points. The LC includes in total 13 transit events. The contamination factor was found to be $L_3 = 2.0 \pm 0.1\%$ by Hébrard et al. (2011).

We observed four transit events in 2014 and 2016 at the OSN. The ground-based as well as the *CoRoT* LCs of CoRoT-18 show brightness bumps that could be attributed to stellar spots. Stellar activity complicates transit mod-

Table 11. Same as Table 5 but for all transits of *CoRoT*-12 b. The O-C was calculated with the ephemeris given in equation 3.

Telescope	Epoch	T_c [BJD _{TDB}]	O-C [min]
CoRoT	0	2454398.6288 ± 0.0017	1.53 ± 2.45
CoRoT	1	2454401.4517 ± 0.0018	-5.88 ± 3.60
CoRoT	2	2454404.2834 ± 0.0023	-0.63 ± 2.16
CoRoT	3	2454407.1119 ± 0.0016	0.01 ± 2.30
CoRoT	4	2454409.9395 ± 0.0024	-0.64 ± 3.89
CoRoT	5	2454412.7744 ± 0.0027	9.22 ± 4.03
CoRoT	6	2454415.5952 ± 0.0028	-1.22 ± 5.47
CoRoT	7	2454418.4242 ± 0.0038	0.14 ± 6.34
CoRoT	8	2454421.2521 ± 0.0044	-0.08 ± 2.16
CoRoT	9	2454424.0803 ± 0.0015	0.13 ± 3.02
CoRoT	10	2454426.9010 ± 0.0017	-10.45 ± 2.45
CoRoT	11	2454429.7375 ± 0.0039	1.71 ± 5.62
CoRoT	12	2454432.5633 ± 0.0037	-1.53 ± 5.33
CoRoT	13	2454435.3948 ± 0.0017	3.43 ± 2.45
CoRoT	14	2454438.2213 ± 0.0017	1.19 ± 2.45
CoRoT	15	2454441.0479 ± 0.0013	-0.90 ± 1.87
CoRoT	16	2454443.8766 ± 0.0013	0.03 ± 2.16
CoRoT	17	2454446.7054 ± 0.0017	1.11 ± 2.45
CoRoT	18	2454449.5330 ± 0.0017	0.46 ± 1.87
CoRoT	19	2454452.3613 ± 0.0015	0.82 ± 2.16
CoRoT	20	2454455.1891 ± 0.0016	0.45 ± 2.30
CoRoT	21	2454458.0163 ± 0.0014	-0.78 ± 2.02
CoRoT	22	2454458.8448 ± 0.0013	-0.13 ± 1.87
CoRoT	23	2454463.6724 ± 0.0016	-0.78 ± 2.45
CoRoT	24	2454466.5004 ± 0.0015	-0.78 ± 2.16
CoRoT	25	2454469.3291 ± 0.0013	-0.86 ± 1.87
CoRoT	26	2454472.1560 ± 0.0014	0.07 ± 2.02
CoRoT	27	2454474.9849 ± 0.0015	-1.59 ± 2.16
CoRoT	28	2454477.8146 ± 0.0015	-0.37 ± 2.16
CoRoT	29	2454480.6407 ± 0.0014	2.01 ± 2.16
CoRoT	30	2454483.4705 ± 0.0015	-0.81 ± 2.02
CoRoT	31	2454486.2966 ± 0.0014	1.71 ± 2.02
CoRoT	32	2454489.1256 ± 0.0013	-1.10 ± 1.87
CoRoT	33	2454491.9530 ± 0.0013	0.26 ± 2.02
CoRoT	34	2454494.7819 ± 0.0017	-0.68 ± 2.45
CoRoT	35	2454497.6113 ± 0.0017	0.54 ± 2.45
CoRoT	36	2454500.4370 ± 0.0013	2.48 ± 2.02
CoRoT	37	2454503.2648 ± 0.0013	-0.90 ± 1.87
CoRoT	38	2454506.0949 ± 0.0013	-0.90 ± 1.87
CoRoT	39	2454506.0949 ± 0.0017	1.68 ± 2.45
CoRoT	40	2454508.9237 ± 0.0016	2.76 ± 2.30
CoRoT	41	2454511.7498 ± 0.0017	2.76 ± 2.45
CoRoT	42	2454514.5773 ± 0.0014	-0.06 ± 2.02
CoRoT	43	2454517.4036 ± 0.0022	-0.85 ± 3.17
CoRoT	44	2454517.4036 ± 0.0021	-0.85 ± 3.02
CoRoT	45	2454517.4036 ± 0.0026	-3.38 ± 3.74
CoRoT	46	2454520.2324 ± 0.0029	-3.38 ± 4.18
CoRoT	925	2454523.0617 ± 0.0020	-2.30 ± 2.88
CoRoT	1041	2454523.0617 ± 0.0019	-2.30 ± 2.74
CoRoT	1077	2454523.0617 ± 0.0013	-0.50 ± 1.87
OSN	925	2454525.8895 ± 0.0013	-0.50 ± 1.87
OSN	1041	2454525.8895 ± 0.0024	-0.87 ± 3.46
OSN	1077	2454528.7215 ± 0.0026	-0.87 ± 3.74
OSN	1077	2454528.7215 ± 0.0032	4.82 ± 4.61
OSN	1077	2454528.7215 ± 0.0035	4.82 ± 5.04
OSN	925	2457014.5746 ± 0.0012	-2.71 ± 1.73
OSN	1041	2457342.6308 ± 0.0013	-2.71 ± 1.87
OSN	1077	2457342.6308 ± 0.0009	0.41 ± 1.27
OSN	1077	2457342.6308 ± 0.0009	0.41 ± 1.30
OSN	1077	2457444.4412 ± 0.0011	1.10 ± 1.58
OSN	1077	2457444.4412 ± 0.0010	1.10 ± 1.44

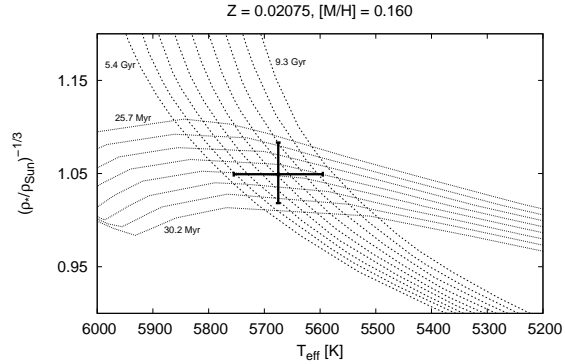


Figure 12. Position of *CoRoT*-12 in the $\rho_A^{-1/3} - T_{\text{eff}}$ plane. The PARSEC isochrones of metallicity $[M/H]=0.16$ for $\log(\text{age}) = 7.41 - 7.48$ with steps of 0.01 and $\log(\text{age}) = 9.73 - 9.97$ with steps of 0.03 for the young and the old age, respectively, are also shown.

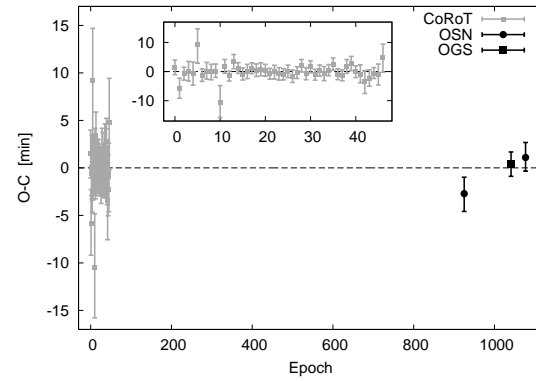


Figure 13. Same as Fig. 3 but for *CoRoT*-12 b. The dashed line represents the updated ephemeris given in equation 3.

elling due to the non-homogeneous brightness distribution on the stellar surface (e.g. Czesla et al. 2009; Oshagh et al. 2013). If occulted and unocculted spots outside the transit path are not correctly modelled, systematic errors in the determination of the system parameters will arise. The detailed spot modelling for *CoRoT*-18 is discussed in Raetz et al. (in preparation). Before the simultaneous transit fitting of all *CoRoT* white light and the ground-based *R*-band transits with TAP we removed all parts of the LCs where spot-features were identified by Raetz et al. (in preparation). The ground-based LCs with the best-fitting model, the simultaneous fit of all *CoRoT* and ground-based LCs and the resulting system parameters are given in Figs. 14 and 15 and Table 4, respectively.

By plotting *CoRoT*-18 in the $\rho_A^{-1/3} - T_{\text{eff}}$ plane (Fig. 16), we confirm the finding of Hébrard et al. (2011) that *CoRoT*-18 is consistent with very young (~ 33 Myr) and old (~ 7 Gyr) ages. The derived physical properties that are summarized in Table 12 agree, on average within $\sim 1.1\sigma$, with the values of Hébrard et al. (2011) and Southworth (2012). We found the largest deviations from the Hébrard et al. (2011) values for the inclination ($\sim 2.4\sigma$), the impact parameter ($\sim 2.8\sigma$), and the stellar density ($\sim 1.9\sigma$). These discrepancies most likely arise from the different treatment of the stellar activity.

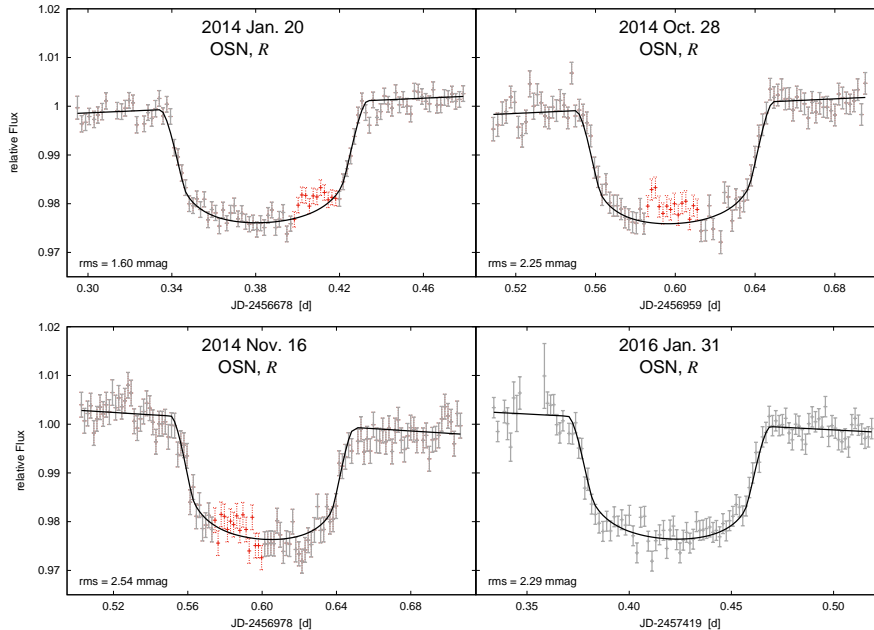


Figure 14. Same as Fig. 2 but for CoRoT-18. The parts of the LC identified as spot features by Raetz et al. (in preparation) shown here as red dashed data points were not used in the analysis (see text). The dates of observation, observatory, filter, and the rms of the fit are indicated in each individual panel.

We used the transit times derived by the simultaneous transit modelling with TAP of the spot removed LCs to refine the ephemeris. Our OSN observations were carried out 4-6 yr after the *CoRoT* discovery. Using the original ephemeris of Hébrard et al. (2011) the calculated transit times deviate from the observed ones by up to ~ 34 min. Within total 17 mid-transit times, we have been able to refine the orbital elements and improve their precision. The result is given in equation 4 ($\chi^2 = 8.4$, reduced $\chi^2 = 0.56$):

$$T_{c[\text{BJD}_{\text{TDB}}]}(E) = (2455321.72565 + E \cdot 1.9000900) \text{ d} \pm 0.00024 \pm 0.0000005 \quad (4)$$

The orbital period P is 1.8 s longer and six times more precise than the one given in Hébrard et al. (2011). The transit times and O-C values are given in Table 13 while Fig. 17 shows the resulting O-C diagram. We could not find indications for TTVs. GLS resulted in a period of $P_{\text{TTV}} = 75.0 \pm 0.2$ epochs with an FAP of 99.8%.

10 COROT-20

CoRoT-20 b is another hot Jupiter that was discovered in the *CoRoT* field SRA03 which was monitored for ~ 24.3 d starting on 2010 March 1 (Deleuil et al. 2012). The ~ 10 mmag deep transit event was detected by the ‘alarm mode’-pipeline which triggered ground-based follow-up observations. Photometric transit observations and RV measurements were carried out at the WISE observatory and with HARPS, SOPHIE, and FIES at the NOT, respectively. The planet orbits its G2-type dwarf with an orbital period of 9.24 d and an eccentricity of 0.56. CoRoT-20 b belongs to the most compact planets known so far. It is an unusual and, hence, a very interesting object as it populates the border of the gap between hot Jupiters and very massive hot Jupiters in the

Table 12. Same as Table 6 but for the CoRoT-18 system. Values derived by Hébrard et al. (2011, H11) and Southworth (2012, S12) are given for comparison.

Parameter	This work	H11	S12
Planetary parameters			
R_b [R_{Jup}]	$1.146 \pm_{0.048}^{0.039}$	1.31 ± 0.18	1.251 ± 0.083
M_b [M_{Jup}]	$3.30 \pm_{0.19}^{0.19}$	3.47 ± 0.38	3.27 ± 0.17
ρ_b [ρ_{Jup}]	$2.06 \pm_{0.29}^{0.24}$	1.65 ± 0.60	1.56 ± 0.30
$\log g_b$	$3.797 \pm_{0.030}^{0.021}$		3.714 ± 0.055
T_{eq} [K]	$1487 \pm_{19}^{19}$	1550 ± 90	1490 ± 45
Θ	$0.189 \pm_{0.020}^{0.019}$		0.173 ± 0.012
Stellar parameters			
R_A [R_{\odot}]	$0.883 \pm_{0.031}^{0.025}$	1.00 ± 0.13	0.924 ± 0.057
M_A [M_{\odot}]	0.88 ± 0.07	0.95 ± 0.15	0.861 ± 0.059
ρ_A [ρ_{\odot}]	$1.28 \pm_{0.09}^{0.04}$	0.96 ± 0.17	1.09 ± 0.16
$\log g_A$	$4.491 \pm_{0.023}^{0.015}$	4.4 ± 0.1	4.442 ± 0.043
$\log \frac{L_A}{L_{\odot}}$	-0.17 ± 0.06		
$\log(\text{Age})$	7.50 ± 0.04		
	9.84 ± 0.26		
Geometrical parameters			
a [au]	0.0288 ± 0.0008	0.0295 ± 0.0016	0.0286 ± 0.0007
i [$^{\circ}$]	$89.9 \pm_{1.6}^{1.6}$	$86.5 \pm_{0.9}^{1.4}$	86.8 ± 1.7
b	$0.01 \pm_{0.20}^{0.20}$	$0.40 \pm_{0.14}^{0.08}$	

period-mass diagram for close-in exoplanets ($P < 10$ d and $M < 15 M_{\text{Jup}}$, see Fig. 8 in Raetz et al. 2015). Because of its relatively long period only three transit events could be observed during the SR. Images of the area around the star

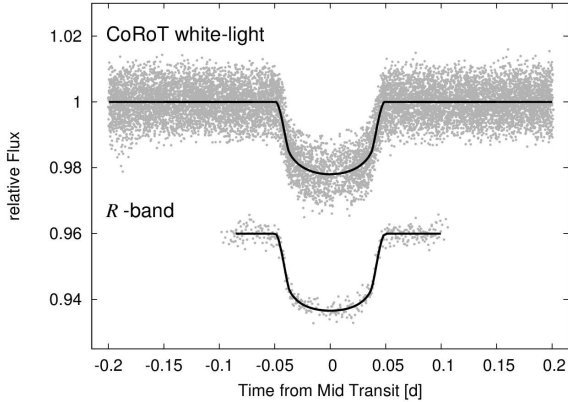


Figure 15. Phase-folded LCs of the 13 *CoRoT* transits as well as of the four OSN *R*-band transits of CoRoT-18. The trend was removed before phase-folding. Overlaid are the best-fitting models obtained with TAP.

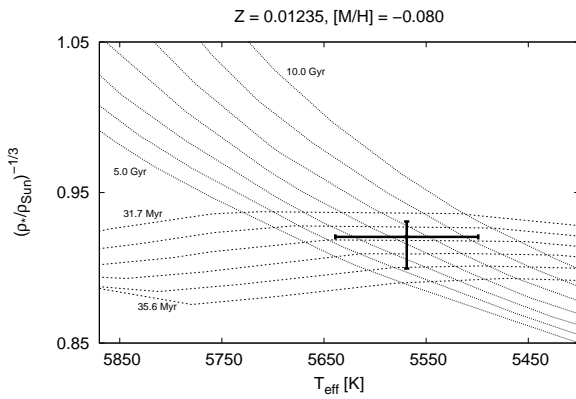


Figure 16. Position of CoRoT-18 in the $\rho_A^{-1/3} - T_{\text{eff}}$ plane. The PARSEC isochrones of metallicity $[M/H] = -0.08$ for $\log(\text{age}) = 7.50 - 7.55$ with steps of 0.01 and $\log(\text{age}) = 9.70 - 10.00$ with steps of 0.05 for the young and the old age, respectively, are also shown.

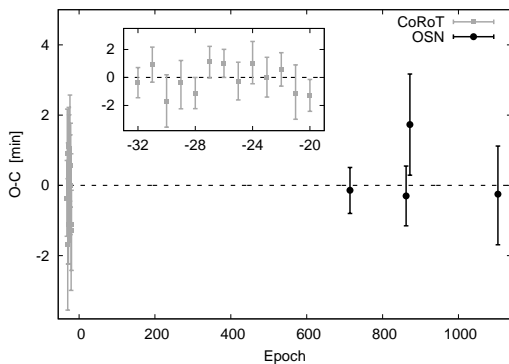


Figure 17. Same as Fig. 3 but for CoRoT-18 b. The dashed line represents the updated ephemeris given in equation 4.

Table 13. Same as Table 5 but for all transits of CoRoT-18 b. The O-C was calculated with the ephemeris given in equation 4. T_c : mid-transit time of the spot removed LCs.

Telescope	Epoch	T_c [BJD _{TDB}]	O-C [min]
CoRoT	-32	$2455260.922523 \pm 0.00074$ 0.00076	-0.3 ± 1.07 1.09
CoRoT	-31	$2455262.823483 \pm 0.00088$ 0.00086	0.9 ± 1.27 1.24
CoRoT	-30	$2455264.721783 \pm 0.00130$ 0.00130	-1.6 ± 1.87 1.87
CoRoT	-29	$2455266.622783 \pm 0.00130$ 0.00130	-0.3 ± 1.58 1.57
CoRoT	-28	$2455268.522353 \pm 0.00078$ 0.00077	-1.1 ± 1.12 1.11
CoRoT	-27	$2455270.423993 \pm 0.00077$ 0.00080	1.1 ± 1.11 1.15
CoRoT	-26	$2455272.324023 \pm 0.00069$ 0.00071	1.0 ± 0.99 1.02
CoRoT	-25	$2455274.223202 \pm 0.00096$ 0.00092	-0.2 ± 1.38 1.32
CoRoT	-24	$2455276.124182 \pm 0.00110$ 0.00100	0.9 ± 1.58 1.44
CoRoT	-23	$2455278.023582 \pm 0.00100$ 0.00097	0.0 ± 1.44 1.40
CoRoT	-22	$2455279.924062 \pm 0.00084$ 0.00082	0.5 ± 1.21 1.18
CoRoT	-21	$2455281.822982 \pm 0.00140$ 0.00130	-1.1 ± 2.02 1.87
CoRoT	-20	$2455283.722962 \pm 0.00079$ 0.00079	-1.2 ± 1.14 1.14
OSN	714	$2456678.389800 \pm 0.00045$ 0.00046	-0.1 ± 0.65 0.66
OSN	862	$2456959.603001 \pm 0.00059$ 0.00059	-0.3 ± 0.85 0.85
OSN	872	$2456978.605317 \pm 0.00100$ 0.00100	1.7 ± 1.44 1.44
OSN	1104	$2457419.424813 \pm 0.00095$ 0.00100	-0.2 ± 1.37 1.44

showed that CoRoT-20 is rather isolated resulting in a very low L_3 of less than 0.6%. The failure of the CoRoT DPU No.1, in 2009 March, reduced the total number of stars observed, while allowing to study more of them with the higher sampling rate. Therefore, all data of CoRoT-20 were acquired in short cadence mode. The white-light LC including the three transit events consists of 56 860 unflagged data points.

We observed two transits of CoRoT-20 b in 2015 January and November, one at the OSN and one partial event at ESA's OGS (see Fig. 18). While the slight eccentricity of our other targets only marginal affected the transit shape, the eccentricity of 0.56 for CoRoT-20 b cannot be neglected in the simultaneous transit modelling. We fixed the eccentricity to the value given in Deleuil et al. (2012). The result of the joint modelling of space- and ground-based LCs is given in Table 4 and shown in Fig. 19. The transit times obtained from the transit fitting given in Table 14 allowed us to re-determine the ephemeris. The result is given in equation 5 ($\chi^2 = 0.69$, reduced $\chi^2 = 0.23$):

$$T_{c[\text{BJD}_{\text{TDB}}]}(E) = (2455266.0016 \pm 0.0010 + E \cdot 9.243180 \pm 0.000009) \text{ d} \quad (5)$$

Fig. 20 shows the O-C diagram created with the updated ephemeris. The orbital period is ~ 28 s higher and 33 times more precise than the one given in Deleuil et al. (2012). With only five measurements we could not find any TTVs. The physical properties are summarized in Table 15. The parameters are in good agreement with the ones of Deleuil et al. (2012). The largest deviation we found is 1.3σ for the planetary density.

CoRoT-20 appears to be a quite star as its LC does not show any features. In addition, the spectra show no signs of chromospheric activity. Because of the measurable Li-line CoRoT-20 is likely a young star in the last stages of the pre-main-sequence phase (Deleuil et al. 2012). Our measurements confirm the age estimate of Deleuil et al. (2012) but

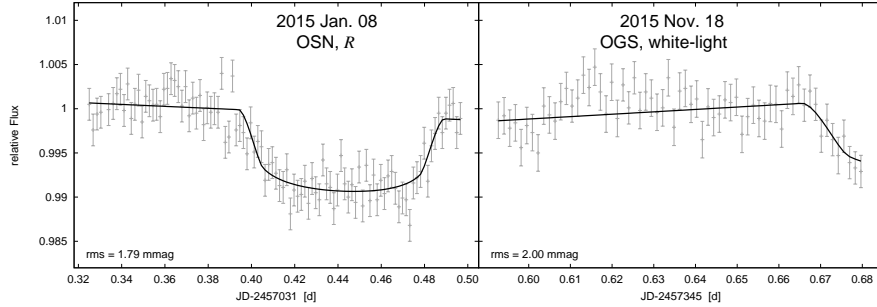


Figure 18. Same as Fig. 2 but for CoRoT-20. The dates of observation, observatory, filter, and the *rms* of the fit are indicated in each individual panel.

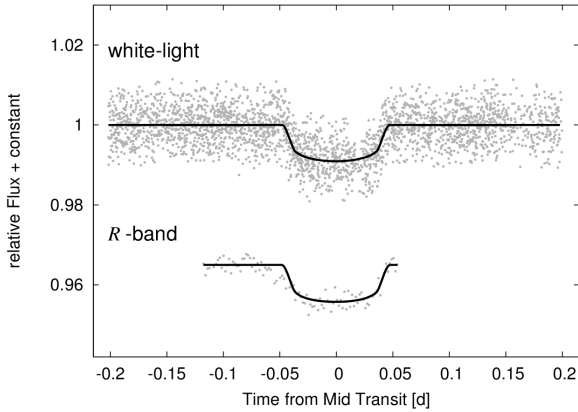


Figure 19. Phase-folded LCs of all three *CoRoT* transits as well as our own transits of CoRoT-20. The trend was removed before phase-folding. Overlaid are the best-fitting models obtained with TAP.

Table 14. Same as Table 5 but for all transits of CoRoT-20 b. The O-C was calculated with the ephemeris given in equation 5.

Telescope	Epoch	T_c [BJD _{TDB}]	O-C [min]
CoRoT	0	$2455266.0011 \pm \begin{smallmatrix} 0.0015 \\ 0.0015 \end{smallmatrix}$	$-0.51 \pm \begin{smallmatrix} 2.16 \\ 2.16 \end{smallmatrix}$
CoRoT	1	$2455275.2452 \pm \begin{smallmatrix} 0.0019 \\ 0.0019 \end{smallmatrix}$	$0.81 \pm \begin{smallmatrix} 2.74 \\ 2.74 \end{smallmatrix}$
CoRoT	2	$2455284.4885 \pm \begin{smallmatrix} 0.0019 \\ 0.0020 \end{smallmatrix}$	$0.97 \pm \begin{smallmatrix} 2.74 \\ 2.88 \end{smallmatrix}$
OSN	191	$2457031.4480 \pm \begin{smallmatrix} 0.0020 \\ 0.0020 \end{smallmatrix}$	$-2.79 \pm \begin{smallmatrix} 2.88 \\ 2.88 \end{smallmatrix}$
OGS	225	$2457345.7182 \pm \begin{smallmatrix} 0.0026 \\ 0.0022 \end{smallmatrix}$	$-0.13 \pm \begin{smallmatrix} 3.74 \\ 3.17 \end{smallmatrix}$

are less precise. The modified HR-diagram together with the PARSEC isochrones can be found in Fig. 21.

11 COROT-27

CoRoT-27 b is a very massive ($M = 10.39 \pm 0.55 M_{Jup}$) transiting planet on a 3.58 d orbit around a 4.2 Gyr-old G2 star (Parviainen et al. 2014). It was detected in the field LRC08 that was observed continuously by *CoRoT* for 83.5 d (from 2011 July 8 to 2011 September 30). It belongs, like CoRoT-20 b, to the densest exoplanets known so far. Although many of the so-called hot super-Jupiters have elliptical orbits, the 13 RV measurements of CoRoT-27 b obtained with HARPS in summer 2012 by Parviainen et al. (2014) do not indicate a

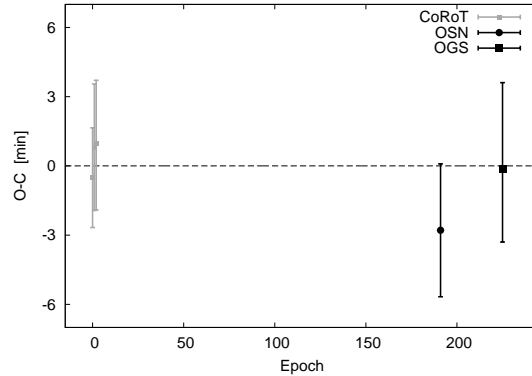


Figure 20. Same as Fig. 3 but for CoRoT-20 b. The dashed line represents the updated ephemeris given in equation 5.

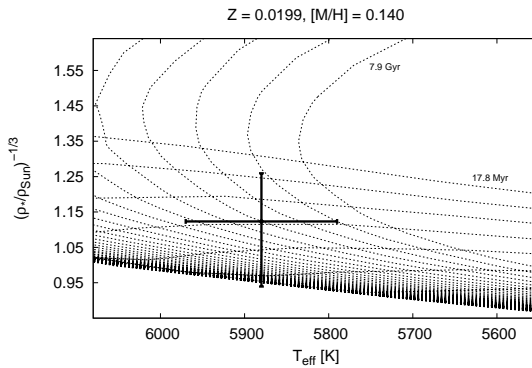


Figure 21. Position of CoRoT-20 in the $\rho_A^{-1/3} - T_{eff}$ plane. The PARSEC isochrones of metallicity $[M/H]=0.14$ for $\log(\text{age}) = 7.25-9.90$ with steps of 0.05 are also shown.

significant non-zero eccentricity. Furthermore, massive close-in planets are mostly found around F-type stars and only rarely around G-stars, as it is the case for CoRoT-27 b. This makes CoRoT-27 b an important target to constrain formation, migration, and evolution of gas giant planets.

We scheduled two transit observations of CoRoT-27 b in 2016 June with OSN. In both cases we obtained good quality LCs covering the whole predicted transit window (predicted using the ephemeris of Parviainen et al. 2014) including out-of-transit data before and after the assumed transit time. In none of the LCs we could detect the transit event. As shown in Fig. 22 the $\sim 1\%$ deep transit event should have easily

Table 15. Same as Table 6 but for the *CoRoT*-20 system. Values derived by Deleuil et al. (2012, D12) and Southworth (2012, S12) are given for comparison.

Parameter	This work	D12	S12
Planetary parameters			
R_b [R_{Jup}]	$1.00 \pm_{0.21}^{0.18}$	0.84 ± 0.04	1.16 ± 0.26
M_b [M_{Jup}]	$4.14 \pm_{0.3}^{0.36}$	4.24 ± 0.23	5.06 ± 0.36
ρ_b [ρ_{Jup}]	$3.9 \pm_{2.4}^{2.1}$	6.67 ± 0.83	3.0 ± 2.5
$\log g_b$	$4.01 \pm_{0.18}^{0.15}$		3.968 ± 0.215
T_{eq} [K]	$1024 \pm_{16}^{16}$	1002 ± 24	1100 ± 150
Θ	$0.67 \pm_{0.17}^{0.16}$		0.70 ± 0.17
Stellar parameters			
R_A [R_{\odot}]	$1.16 \pm_{0.20}^{0.15}$	1.02 ± 0.05	1.34 ± 0.37
M_A [M_{\odot}]	1.10 ± 0.1	1.14 ± 0.08	1.11 ± 0.01
ρ_A [ρ_{\odot}]	$0.71 \pm_{0.35}^{0.26}$	$1.071 \pm_{0.037}^{0.932}$	0.46 ± 0.48
$\log g_A$	$4.35 \pm_{0.14}^{0.11}$	4.20 ± 0.15	4.23 ± 0.24
$\log \frac{L_A}{L_{\odot}}$	0.17 ± 0.18		
$\log(\text{Age})$	8.6 ± 1.4	$8.00 \pm_{0.22}^{0.95}$	
Geometrical parameters			
a [au]	0.0891 ± 0.0038	0.0902 ± 0.0021	0.0892 ± 0.0028
i [°]	$85.9 \pm_{2.2}^{2.5}$	88.21 ± 0.53	83.5 ± 3.8
b	$0.6 \pm_{0.3}^{0.4}$	0.26 ± 0.08	

been detected. The dashed lines in Fig. 22 give the range of the transit beginning and end times expected from the uncertainties in the ephemeris of Parviainen et al. (2014). The non-detection indicates that the original determined orbital period was not accurate enough to predict the transit event 5 yr later. Our LCs provide a lower limit for the deviation from the predicted transit time. The non-detection in our observations means that the transit must have happened at least 3.9 h too early or 4.5 h too late. To give some constraints on the orbital period, we analysed the *CoRoT* observations. To determine the range of periods that is excluded by our observations we carried out two individual weighted linear fits, one with the earliest possible transit mid-time after our observed window (transit 4.5 h too late in respect to the original ephemeris) and the other with the latest possible transit mid-time before our observations (transit 3.9 h too early). Equations 6 and 7 give a lower limit for a longer period and an upper limit for a shorter period, respectively.

$$T_{c[\text{BJD}_{\text{TDB}}]}(E) = (2455748.6810 + E \cdot 3.575712) \text{ d} \quad (6)$$

$$T_{c[\text{BJD}_{\text{TDB}}]}(E) = (2455748.6905 + E \cdot 3.575004) \text{ d} \quad (7)$$

Hence, we can exclude periods between 3.575004 d and 3.575712 d with our observations. However, the χ^2 values of 37.8 and 5.3 for equation 6 and equation 7, respectively, suggest, that a shorter period might be more likely. Therefore, photometric monitoring of *CoRoT*-27 a few hours before the predicted transit window is essential to recover the passage of this very interesting exoplanet in front of its host star.

As we could not add new transit events and, hence could not add new information, we did not re-determine the physical properties of *CoRoT*-27.

12 SUMMARY AND CONCLUSIONS

In our project to follow-up with ground-based photometry transiting planets discovered by the *CoRoT* space telescope, we observed five systems between 2012 and 2016. The aim of our investigation has been to refine their orbital elements, constrain their physical parameters and search for additional bodies in the system. *CoRoT*-5, *CoRoT*-8, *CoRoT*-12, *CoRoT*-18, *CoRoT*-20, and *CoRoT*-27 were selected on the basis of their observability and expected photometric precision, of their at least slightly non-zero eccentricity (or little information to constrain the eccentricity) and /or of the uncertainties on their original published ephemeris.

Since *CoRoT* could observe transiting planets continuously only for a maximum duration of 150 d, the observations of our selected targets are well suited for our objectives because, on average, they took place 7 yr after the exoplanet discovery. In total, we observed 14 transit events for five out of six targets. Despite the observation of two high precision LCs, we could not detect the expected transit of *CoRoT*-27 b.

To conduct a homogeneous analysis of all available transit LCs, we re-analysed the observations of *CoRoT*. We extracted all transit events, normalised, and cleaned (outlier removal) the LCs. With a total of 34, 25, 50, 17, and five transits for *CoRoT*-5 b, *CoRoT*-8 b, *CoRoT*-12 b, *CoRoT*-18 b, and *CoRoT*-20 b, respectively, we performed simultaneous transit fitting in order to determine the system parameters. These were then used to calculate stellar, planetary and geometrical parameters of the systems. Our results for *CoRoT*-5 b, *CoRoT*-8 b, *CoRoT*-12 b, *CoRoT*-18 b, and *CoRoT*-20 b plotted in a mass-radius diagram for transiting exoplanets are shown in Fig. 23. *CoRoT*-5 b is the planet with the lowest density, and *CoRoT*-8 b the one with the lowest mass and radius in our sample. Approximately 70% of the Jupiter-like transiting exoplanets ($M > 0.5 M_{\text{Jup}}$) have a density between 0.2 and 1.2 ρ_{Jup} . Therefore, *CoRoT*-5 b, *CoRoT*-8 b, and *CoRoT*-12 b have a comparable density to the majority of the transiting planets. *CoRoT*-18 b and *CoRoT*-20 b show a higher density. Only 8% of the Jupiter-like transiting exoplanets have a higher density than *CoRoT*-20 b. Hence, our measurements confirm that *CoRoT*-20 b is one of the most compact planets known so far.

In most cases, our determined physical properties are in agreement with values reported in previous studies. For *CoRoT*-5, we found that the geometrical parameters are in excellent agreement, while the stellar and planetary values agree within the error bars on a 2σ level. Also for *CoRoT*-12 and *CoRoT*-20, we found our derived physical properties in excellent (average deviation $\sim 0.5\sigma$) and in good agreement (average deviation $\sim 1.0\sigma$), respectively, with a largest deviation of 1.25σ . Only for *CoRoT*-8 and *CoRoT*-18, we found slight deviations from the literature values. In the case of *CoRoT*-18 this most likely arises from the different treatment of the stellar activity. For *CoRoT*-8 our LC derived stellar density is significant lower (on a 5σ level). The reason for these discrepancies were found to be strong parameter correlations in our LC modelling, which implies, e.g., that a smaller radius can be accounted for with a higher inclination i without degrading the quality of the fit. By using a prior on the stellar density we derived physical properties that are in good agreement with the literature values.

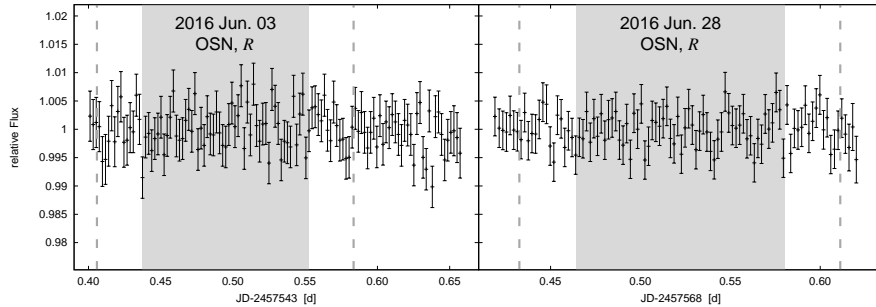


Figure 22. LCs of CoRoT-27. The grey area indicates the predicted transit window. The dashed lines give the transit beginning and end including the uncertainties of the ephemeris given in Parviainen et al. (2014). The transit event was not detected. The date of observation, observatory, and filter are indicated in each individual panel.

More high precision follow-up observations would be needed to break the degeneracies between the parameters. In five out of six cases the observed mid-transit times deviate from the expected values more than estimated from the uncertainties on the original published ephemeris. One explanation is that the short observational baseline of *CoRoT* does not allow for a precise determination of the orbital elements, and therefore the uncertainties on the original ephemeris were underestimated. For the CoRoT-27 system we could not even recover the transit event in the observing window predicted by the published ephemeris. The non-detection in our observations means that the transit must have happened at least 3.9 h earlier or 4.5 h later. Our analysis of the *CoRoT*-transits suggests that the orbital period might be shorter than the literature one. Hence, the confirmation of our finding would require to re-observe the system a few hours before the original transit time predictions. In the five remaining systems, CoRoT-5, CoRoT-8, CoRoT-12, CoRoT-18 and CoRoT-20, our re-determination of the orbital periods resulted in values that are between 0.9 and 29 s longer and between 1.2 and 33 times more precise than the literature periods. Although some systems show a correlated structure of their transit times, we could not find significant periodicities in the timing residuals (FAP $\sim 99\%$ in all cases). A structured O-C diagram may also be caused by stellar activity.

Our ground-based photometric follow-up observations have allowed us to improve the transit time predictions for six targets. In the era of space-based exoplanet characterization, accurate transit times are imperative for an efficient use of the observing time of future missions, like CHEOPS or JWST.

ACKNOWLEDGEMENTS

We would like to thank H. Gilbert for participating in some of the observations at the University Observatory Jena. SR acknowledge support from the People Programme (Marie Curie Actions) of the European Union’s Seventh Framework Programme (FP7/2007-2013) under REA grant agreement no. [609305]. MF acknowledges financial support from grants AYA2014-54348-C3-1-R, AYA2011-30147-C03-01 and AYA2016-79425-C3-3-P of the Spanish Ministry of Economy and Competivity (MINECO), co-funded with EU FEDER funds. CM acknowledges support from the DFG through

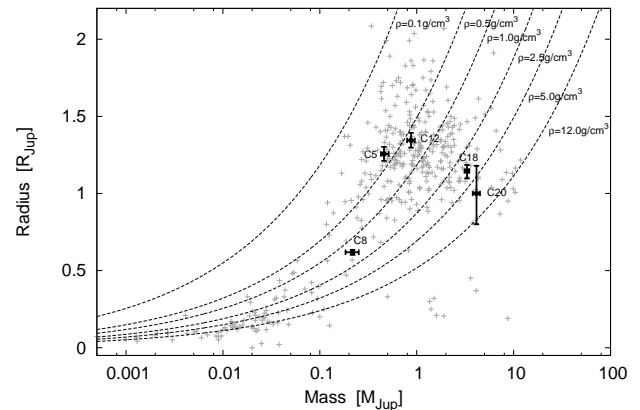


Figure 23. Mass-Radius diagram for transiting exoplanets, with our results for CoRoT-5 b, CoRoT-8 b, CoRoT-12 b, CoRoT-18 b, and CoRoT-20 b. The lines of constant density (dashed lines) are also given.

grant SCHR665/7-1. The present study was made possible thanks to observations obtained with *CoRoT*, a space project operated by the French Space Agency, CNES, with participation of the Science Program of ESA, ESTEC/RSSD, Austria, Belgium, Brazil, Germany, and Spain. This research was (partly) based on data obtained at the 1.5m telescope of the Sierra Nevada Observatory (Spain), which is operated by the Consejo Superior de Investigaciones Científicas (CSIC) through the Instituto de Astrofísica de Andalucía.

REFERENCES

- Akeson R. L., Chen X., Ciardi D., Crane M., Good J., Harbut M., Jackson E., Kane S. R., et al. 2013, *PASP*, 125, 989
- Angus R., Aigrain S., Foreman-Mackey D., McQuillan A., 2015, *MNRAS*, 450, 1787
- Auvergne M., Bodin P., Boissard L., Buey J.-T., Chain-treuil S., Epstein G., Joutet M., Lam-Trong T., et al. 2009, *A&A*, 506, 411
- Batalha N. M., Borucki W. J., Bryson S. T., Buchhave L. A., Caldwell D. A., Christensen-Dalsgaard J., Ciardi D., Dunham E. W., et al. 2011, *ApJ*, 729, 27

- Bordé P., Bouchy F., Deleuil M., Cabrera J., Jorda L., Lovis C., Csizmadia S., Aigrain S., et al. 2010, *A&A*, 520, A66
- Bressan A., Marigo P., Girardi L., Salasnich B., Dal Cero C., Rubele S., Nanni A., 2012, *MNRAS*, 427, 127
- Broeg C., Fernández M., Neuhäuser R., 2005, *Astronomische Nachrichten*, 326, 134
- Carter J. A., Winn J. N., 2009, *ApJ*, 704, 51
- Chaintreuil S., Deru A., Baudin F., Ferrigno A., Grolleau E., Romagnan R., 2016, II.4 The "ready to use" CoRoT data. p. 61
- Claret A., 2000, *A&A*, 363, 1081
- CoRoT Team 2016, *The CoRoT Legacy Book: The adventure of the ultra high precision photometry from space, by the CoRoT Team*
- Csizmadia S., Pasternacki T., Dreyer C., Cabrera J., Erikson A., Rauer H., 2013, *A&A*, 549, A9
- Czesla S., Huber K. F., Wolter U., Schröter S., Schmitt J. H. M. M., 2009, *A&A*, 505, 1277
- Deleuil M., Bonomo A. S., Ferraz-Mello S., Erikson A., Bouchy F., Havel M., Aigrain S., Almenara J.-M., et al. 2012, *A&A*, 538, A145
- Deleuil M., Meunier J. C., Moutou C., Surace C., Deeg H. J., Barbieri M., Deboscher J., Almenara J. M., et al. 2009, *AJ*, 138, 649
- Eastman J., Gaudi B. S., Agol E., 2013, *PASP*, 125, 83
- Eastman J., Siverd R., Gaudi B. S., 2010, *PASP*, 122, 935
- Ehrenreich D., Désert J.-M., 2011, *A&A*, 529, A136
- Evans D. F., Southworth J., Maxted P. F. L., Skottfelt J., Hundertmark M., Jørgensen U. G., Dominik M., Alsubai K. A., et al. 2016, *A&A*, 589, A58
- Gaia Collaboration Brown A. G. A., Vallenari A., Prusti T., de Bruijne J. H. J., Babusiaux C., Bailer-Jones C. A. L., Biermann M., Evans D. W., Eyer L., et al. 2018, *A&A*, 616, A1
- Gaia Collaboration Prusti T., de Bruijne J. H. J., Brown A. G. A., Vallenari A., Babusiaux C., Bailer-Jones C. A. L., Bastian U., Biermann M., Evans D. W., et al. 2016, *A&A*, 595, A1
- Gazak J. Z., Johnson J. A., Tonry J., Dragomir D., Eastman J., Mann A. W., Agol E., 2012, *Advances in Astronomy*, 2012
- Gillon M., Hatzes A., Csizmadia S., Fridlund M., Deleuil M., Aigrain S., Alonso R., Auvergne M., et al. 2010, *A&A*, 520, A97
- Hébrard G., Evans T. M., Alonso R., Fridlund M., Ofir A., Aigrain S., Guillot T., Almenara J. M., et al. 2011, *A&A*, 533, A130
- Maciejewski G., Niedzielski A., Wolszczan A., Nowak G., Neuhäuser R., Winn J. N., Deka B., Adamów M., et al. 2013, *AJ*, 146, 147
- Mandel K., Agol E., 2002, *ApJL*, 580, L171
- Mugrauer M., Berthold T., 2010, *Astronomische Nachrichten*, 331, 449
- Ollivier M., Deru A., Chaintreuil S., Ferrigno A., Baglin A., Almenara J.-M., Auvergne M., Barros S., et al. 2016, II.2 Description of processes and corrections from observation to delivery. p. 41
- Oshagh M., Santos N. C., Boisse I., Boué G., Montalto M., Dumusque X., Haghhighipour N., 2013, *A&A*, 556, A19
- Parviainen H., Deeg H. J., Belmonte J. A., 2013, *A&A*, 550, A67
- Parviainen H., Gandolfi D., Deleuil M., Moutou C., Deeg H. J., Ferraz-Mello S., Samuel B., Csizmadia S., et al. 2014, *A&A*, 562, A140
- Queloz D., Bouchy F., Moutou C., Hatzes A., Hébrard G., Alonso R., Auvergne M., Baglin A., et al. 2009, *A&A*, 506, 303
- Raetz S., Fernandez M., Marka C., Heras A. M., Maciejewski G., 2015, in *European Physical Journal Web of Conferences Vol. 101 of European Physical Journal Web of Conferences, A transit timing analysis with combined ground- and space-based photometry.* p. 06054
- Raetz S., Maciejewski G., Ginski C., Mugrauer M., Berndt A., Eisenbeiss T., Adam C., Raetz M., et al. 2014, *MNRAS*, 444, 1351
- Raetz S., Maciejewski G., Seeliger M., Marka C., Fernández M., Güver T., Göğüş E., Nowak G., et al. 2015, *MNRAS*, 451, 4139
- Raetz S., Schmidt T. O. B., Czesla S., Klocová T., Holmes L., Errmann R., Kitzke M., Fernández M., et al. 2016, *MNRAS*, 460, 2834
- Rauer H., Queloz D., Csizmadia S., Deleuil M., Alonso R., Aigrain S., Almenara J. M., Auvergne M., et al. 2009, *A&A*, 506, 281
- Safronov V. S., 1972, *Evolution of the protoplanetary cloud and formation of the earth and planets.*
- Schulz R., Erd C., Guilbert-Lepoutre A., Heras A., Raetz S., Smit H., Stankov A., 2014, in *AAS/Division for Planetary Sciences Meeting Abstracts Vol. 46 of AAS/Division for Planetary Sciences Meeting Abstracts, Monitoring of Comets and Extra-Solar Planets with ESA's Optical Ground Station.* p. 214.05
- Sing D. K., 2010, *A&A*, 510, A21
- Southworth J., 2009, *MNRAS*, 394, 272
- Southworth J., 2011, *MNRAS*, 417, 2166
- Southworth J., 2012, *MNRAS*, 426, 1291
- Winn J. N., 2010, *ArXiv e-prints*
- Zechmeister M., Kürster M., 2009, *A&A*, 496, 577